

GEOCHEMISTRY

Heavy boron isotopes in intraplate basalts reveal recycled carbonate in the mantle

Rong Xu^{1*}, Yue Cai^{2*}, Sarah Lambart³, Chunfei Chen⁴, Jun-Bo Zhang⁵, Mei-Fu Zhou¹, Jia Liu⁶, Zhongjie Bai¹, Tao Wu⁷, Feng Huang⁸, Ting Ruan², Yongsheng Liu⁴

Recycling of surficial volatiles such as carbon into the mantle plays a fundamental role in modulating Earth's habitability. However, slab devolatilization during subduction could prevent carbon from entering the deep mantle. Boron isotopes are excellent tracers of recycled volatiles, but correlations between boron isotopes and mantle heterogeneity indicators are rarely observed, thereby casting doubt that substantial amounts of volatiles and boron can be recycled into the deep mantle. Here, we show that boron isotopes in two different types of primitive continental intraplate basalts correlate well with mantle heterogeneity indicators, indicating contributions of various subducted crustal components. A common high- $\delta^{11}\text{B}$ component shared by both types of basalts is best explained as recycled subducted carbonate rather than serpentinite. Our findings demonstrate that subducted carbonate carries heavy B into Earth's deep mantle, and its recycling could account for the high- $\delta^{11}\text{B}$ signatures observed in intraplate magmas and deeply sourced carbonatites.

INTRODUCTION

Recycling of surficial materials, especially carbonates, into the deep mantle at subduction zones plays a fundamental role in modulating the habitability of Earth (1) and in modifying the composition of the deep mantle (2, 3). Recycled crustal components have been identified using many geochemical tracers in ocean island basalts (OIBs) and, to a lesser extent, in mid-ocean ridge basalts (MORBs) (4, 5). However, most geochemical tracers have multiple controlling factors. For example, elemental contents and ratios can be affected by the nature of the mantle components as well as different degrees of partial melting (6, 7); radiogenic isotopes, on the other hand, are affected by both the timing and extent of mantle enrichment or depletion. Volatiles in the mantle such as carbon and water are particularly difficult to trace because of their disproportionate impact on mantle melting (8) and on the partition coefficients of various elements (9, 10). In particular, the involvement of recycled sedimentary carbonate in the petrogenesis of intraplate basalts remains a subject of debate because most previous geochemical tracers cannot directly distinguish recycled carbonates from silicates with ghost carbonate signatures (11–13). For instance, carbonate-silicate interactions at subduction zones may exhaust recycled carbonates and transfer metal cations such as Mg, Zn, and Ca along with their anomalous isotope compositions into silicate minerals of decarbonated eclogites (11, 14). As a result, both recycled carbonates and

decarbonated eclogite may explain anomalous metal isotope compositions of intraplate basalts, leaving open the question regarding the recycling of crustal carbon into the deep mantle.

Boron (B) is a fluid-mobile element that behaves as an incompatible trace element during mantle melting and melt fractionation, with a similar partition coefficient to Nb and Ce (15). Boron isotopes are promising tracers of volatile recycling in the deep mantle (16, 17) because of the large isotopic fractionation between its two stable isotopes, ^{10}B and ^{11}B , that only occurs in near-surface environments (18, 19). B isotopes are typically expressed as $\delta^{11}\text{B}$, the per mil difference between the $^{11}\text{B}/^{10}\text{B}$ ratio of the sample and the NBS 951 boric acid standard. It has been established that $\text{B}(\text{OH})_3$ is the predominant aqueous B species over a wide range of P - T -pH conditions during slab dehydration, which should preferentially incorporate ^{11}B (20). Globally, arc lavas farther away from the trench have gradually lower B/Nb (from ~ 70 to 0.02) and $\delta^{11}\text{B}$ values (from +16 to -10‰) (21–24). In comparison, fresh MORBs have B/Nb values that range from 0.15 to 1.05 and $\delta^{11}\text{B}$ values that range from -3.3 to -9.8‰ (Fig. 1), with an average $\delta^{11}\text{B}$ value of $-7.1 \pm 0.9\text{‰}$ (15). These observations suggest that the residual slab should become progressively lighter in B isotopes during subduction (21, 25–27).

Because of subduction dehydration, both the recycled residual oceanic crust and sediments should have relatively low B contents and $\delta^{11}\text{B}$ values. However, recycled carbonates may be able to preserve their elevated $\delta^{11}\text{B}$ values because of their relatively low water content (28–32). If this is the case, then some OIBs, especially HIMU-type [HIMU stands for high time-integrated μ ($^{238}\text{U}/^{204}\text{Pb}$) or elevated $^{206}\text{Pb}/^{204}\text{Pb}$] (2), should show elevated $\delta^{11}\text{B}$ values that correlate with tracers of recycled carbonate such as elevated Zn isotopes (33). However, boron isotope studies of oceanic basalts (MORBs and OIBs) are often under the suspicion of seawater alteration, given the high B concentration ($\sim 4.5 \mu\text{g/g}$) and elevated $\delta^{11}\text{B}$ ($\sim 39.6\text{‰}$) in seawater (34). Even melt inclusions may be susceptible to the effects of hydrothermal alteration, generating values that could be either too high or too low depending on the assimilated material (35). After screening for signs of seawater alteration, the known ranges of $\delta^{11}\text{B}$ values are -13.7 to -5.8‰ for HIMU-type OIBs represented by La Palma and St. Helena islands (36, 37)

¹State Key Laboratory of Critical Mineral Research and Exploration, Institute of Geochemistry, Chinese Academy of Sciences, Guiyang 550081, China. ²State Key Laboratory of Palaeobiology and Stratigraphy, Nanjing Institute of Geology and Palaeontology, Chinese Academy of Sciences, Nanjing 210008, China. ³Geology and Geophysics, University of Utah, Salt Lake City, UT, USA. ⁴State Key Laboratory of Geological Processes and Mineral Resources, School of Earth Sciences, China University of Geosciences, Wuhan 430074, China. ⁵YU-CUGW Joint Research Center on Deep Earth and Surface Dynamic Coupling, College of Resources and Environment, Yangtze University, Wuhan 430100, China. ⁶Key Laboratory of Geoscience Big Data and Deep Resource of Zhejiang Province, School of Earth Sciences, Zhejiang University, Hangzhou 310027, China. ⁷Ocean College, Zhejiang University, Zhoushan 316021, China. ⁸State Key Laboratory of Geological Processes and Mineral Resources, School of Earth Science and Resources, China University of Geosciences, Beijing 100083, China.

*Corresponding author. Email: xurong@mail.gyig.ac.cn (R.X.); merrycai@gmail.com (Y.C.)

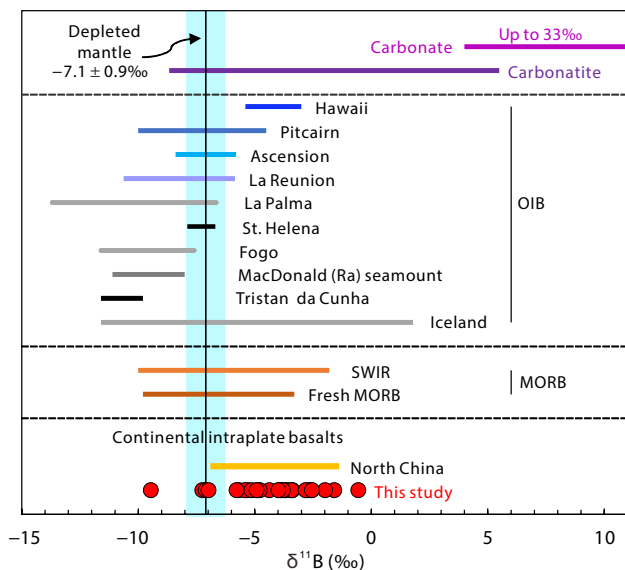


Fig. 1. Ranges of $\delta^{11}\text{B}$ of the depleted mantle, MORBs, OIBs, continental intraplate basalts, carbonatites, and carbonates. The vertical black line is the average depleted mantle value, and the light blue field is the $\delta^{11}\text{B}$ range of mantle (15). Data source: Hawaii (110), La Palma (Canary Island) and La Reunion Island (Piton de Caille) (37), Pitcairn Island, Tristan da Cunha, St. Helena, Ascension Island, the MacDonald Seamount, and Fogo (Cape Verde Islands) (36), Iceland MORB (35, 38), Southwestern Indian Ridge (SWIR) MORB (111), fresh MORB (15), carbonatites (91, 92), carbonates (28–31), and North China continental intraplate basalts (112).

and -11.6 to -3.7‰ for OIBs with mixed source domains such as Iceland and Hawaii (35, 38). While some OIBs do show $\delta^{11}\text{B}$ values slightly higher than the average value of MORBs (Fig. 1), it has been difficult to identify the recycled components using B isotopes because of the lack of clear correlations between B isotopes and mantle heterogeneity indicators. Therefore, the extent to which the B geochemistry of intraplate basalts reflects the incorporation of subducted components in their sources remains unclear.

Boron isotopes of continental intraplate basalts, on the other hand, are much less likely to be altered by weathering because of the much lower B concentration in meteoric waters (39). Therefore, boron isotopes in continental intraplate basalts could contribute to our understanding of volatile cycling in the deep mantle. Cenozoic continental intraplate basalts in the Zhejiang area from southeast (SE) China can be grouped into two types on the basis of their age and composition. The early-stage [~ 26 to 17 million years (Ma) ago] basalts show a stronger influence of the deeply recycled carbonated oceanic crust with elevated ratios of light to heavy rare-earth elements (e.g., La/Yb) and high $\delta^{56}\text{Fe}$ and $\delta^{66}\text{Zn}$ values, while the latter-stage basalts ($< \sim 11$ Ma ago) show signatures of shallow subduction-modified subcontinental lithospheric mantle (SCLM) (40–45). Here, we report high-precision B isotope and concentration analyses on these well-characterized primitive continental intraplate basalts. In combination with elemental abundances and Nd, Sr, Zn, and Fe isotopes (40, 41), these B data demonstrate that heavy B isotopic signatures in crustal carbonates may survive the dehydration process during plate subduction and be recycled into the deep mantle source of intraplate magmas.

Background and samples

Seismological studies have revealed that the subducted western Pacific plate is currently horizontally stagnant in the mantle transition zone (MTZ), extending far (> 1000 km) beyond the present-day Japan-Izu-Bonin-Mariana subduction zone, forming the big mantle wedge beneath eastern China (46). Rather than being associated with an active subduction, the widespread intraplate magmatism in eastern China is thus controlled primarily by melting processes within the big mantle wedge, aided by fluids/melts derived from the stagnant Pacific plate in the MTZ, where the subducted carbonated oceanic crust likely plays a crucial role (47–51). Samples selected for this study are relatively primitive basalts ($\text{MgO} > \sim 8$ wt %) from the Zhejiang area in SE China (40, 42, 43, 45) that have only fractionated olivine, which allows them to preserve signatures of their mantle source. These basalts can be divided into two distinct groups on the basis of age, location, and composition. The early-stage (~ 26 to 17 Ma ago) Oligocene to late-Miocene basalts are predominantly nephelinites and basanites from the inland area, whereas the late-stage late-Miocene and younger basalts ($< \sim 11$ Ma ago) include basanites, alkali basalts, and tholeiites (40, 42). Relative to the late-stage basalts, the early-stage basalts have overall low SiO_2 , high alkali ($\text{Na}_2\text{O} + \text{K}_2\text{O}$), incompatible trace element contents, high $\text{CaO}/\text{Al}_2\text{O}_3$ ratios, strong incompatible element enrichment (e.g., La/Sm), high ratios of light to heavy rare-earth elements (e.g., La/Yb), and high $\delta^{66}\text{Zn}$ and $\delta^{56}\text{Fe}$ values. Thermobarometry analysis, trace element characteristics, and geophysical evidence collectively indicate that the early-stage magmas originated from deeper sources in the asthenosphere, while the late-stage magmas were derived from shallower depths involving both the asthenospheric and lithospheric mantles (40). The details of geological setting, sampling strategy, petrology, major and trace element abundances, and Zn-Fe-Sr-Nd isotope compositions can be found in studies of Xu *et al.* (40, 41). On the basis of these studies, the nature of their mantle sources has been characterized. In the Sr-Nd isotopic space, three mantle components can be identified (fig. S1): (i) a carbonated-pyroxenite, characterized by high $\delta^{66}\text{Zn}$ (40) and $\delta^{56}\text{Fe}$ (41) and moderately enriched Sr and Nd isotopic compositions; (ii) a subduction-modified SCLM, characterized by highly radiogenic Sr and Nd isotopic compositions; and (iii) a depleted asthenospheric component with more depleted Sr and Nd isotopic compositions (40, 41). For clarity, we use the term “enriched” to refer to lava compositions with higher incompatible/compatible element ratios and $^{87}\text{Sr}/^{86}\text{Sr}$ ratios and lower $^{143}\text{Nd}/^{144}\text{Nd}$ ratios than the average normal MORBs (N-MORBs) and “depleted” for the opposite (52). Many previous studies using trace element and isotope analyses have found that the mantle sources of continental intraplate basalts from eastern China are relatively “enriched” and may contain recycled crustal components [e.g., (40, 41, 43, 44, 49, 53–71)]. The intraplate volcanism in the Zhejiang area was most likely triggered by edge-driven small-scale convection related to the variations in the thickness of the lithosphere (40).

The early-stage low-silica basalts likely represent low-degree partial melts of the asthenospheric mantle that preferentially sampled a fusible carbonated eclogite/pyroxenite component at greater depths. Because of the lid effect of the thick lithosphere under the inland area, the melting degree of the depleted mantle would be limited, thereby helping to preserve the enriched isotope signatures, in particular the high $\delta^{66}\text{Zn}$ and $\delta^{56}\text{Fe}$ ratios, and trace element signatures of the more fusible carbonated eclogite. The

late-stage magmatism predominantly occurred along the coast area, where the lithospheric thickness is thinner, which leads to higher degrees of decompression melting and more dilution from melts produced by the depleted asthenospheric mantle. As decompression melting progresses to shallower levels, subsequent melting of the lower part of the metasomatized lithospheric mantle can account for the elemental as well as isotopic signatures of the coastal late-stage basalts (higher SiO_2 , K/U, Sr/Ce, lower La/Yb, enriched Sr and Nd isotopes, etc.). As these continental intraplate basalts represent mixtures of melts from different mantle components, correlations between $\delta^{11}\text{B}$ and other mantle heterogeneity indicators in them (Figs. 2 to 4) can place additional constraints on the

nature of the mantle components involved, such as their devolatilization history.

RESULTS AND DISCUSSION

The measured $\delta^{11}\text{B}$ values range from -9.46 to -2.54 ‰ for the early-stage basalts and from -5.78 to -0.55 ‰ for the late-stage basalts (table S1 and fig. S2), which extend well beyond the range of depleted mantle (-7.1 ± 0.9 ‰) (15). The $\delta^{11}\text{B}$ values of both the early- and late-stage basalts correlate negatively with SiO_2 , Sr/Ce, and Ti/Eu and positively with La/Yb and Ce/Pb, albeit with slightly different slopes, while both groups converge toward a common $\delta^{11}\text{B}$

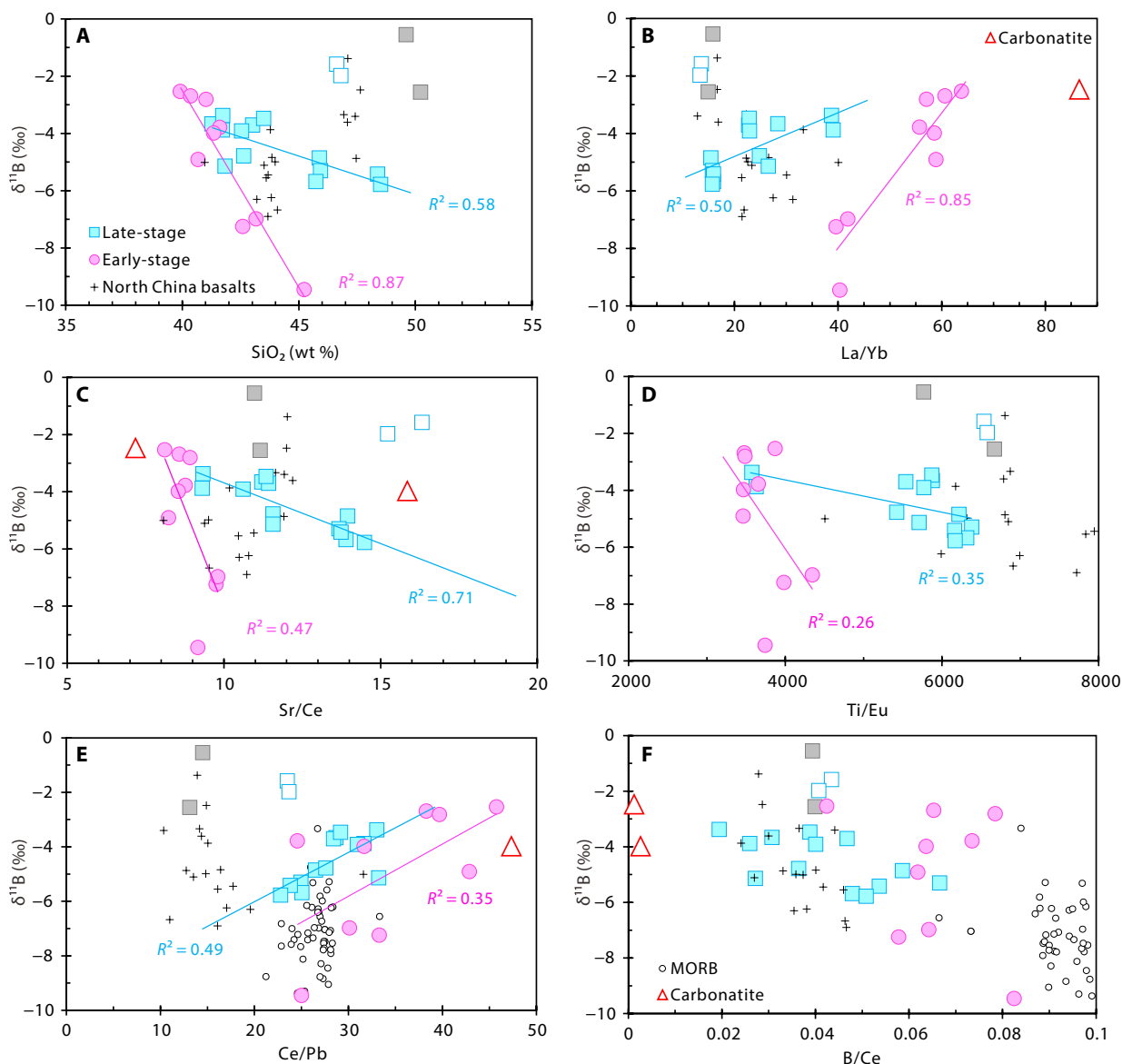


Fig. 2. Boron isotope and concentration data versus elemental tracers of mantle dynamics. $\delta^{11}\text{B}$ variation as a function of (A) SiO_2 , (B) La/Yb, (C) Sr/Ce, (D) Ti/Eu, (E) Ce/Pb, and (F) B/Ce of the studied basalts. The best-fit regressions with R^2 values are shown. For the late-stage samples, four samples (open and gray squares) with the highest $\delta^{11}\text{B}$ are excluded from the regression (see details in Results and Discussion). Data sources: North China basalts (109), fresh MORB (15), and two carbonatites associated with recycled crustal carbon (92).

end-member of -2% (Fig. 2). The late-stage basalts also show strong correlations between B enrichment (B/Ce or B/Nb) and signatures of contribution from a metasomatized SCLM (elevated Sr/Ce and K/U) (Fig. 3).

Four samples of the late-stage basalts with the lowest B concentrations (1.65 to 2.07 parts per million versus 2.13 to 12.56 parts per million for other samples) have the highest $\delta^{11}\text{B}$ values and fall off the general trends delineated by the other samples (Fig. 3). The petrogenesis of two of these outliers (open white squares) is discussed in detail below. The two other outliers (gray squares) were previously identified as having been affected by crustal contamination (40) and are included in this study to constrain the effects of crustal assimilation on the B geochemistry. A more detailed evaluation of the potential effects of crustal contamination and low-temperature alteration can be found in Materials and Methods. Except for these samples, all studied samples show a limited range of Nb/U and Ce/Pb ratios that are well within or above the range of N-MORBs (52) with positive linear correlations between B and Zr contents ($R^2 = 0.83$, $n = 26$), which suggest minimal effects of crustal assimilation and weathering (fig. S2).

Mantle source control of B isotopes

A mantle source control on the B isotope signature of the studied intraplate basalts is corroborated by the correlations between measured $\delta^{11}\text{B}$ values and various indicators of mantle partial melting

and source heterogeneity, including SiO_2 , La/Yb, Sr/Ce, Ti/Eu, Ce/Pb, and $\delta^{66}\text{Zn}$ ratios (Figs. 2 to 4). As the equilibrium fractionation of B isotope is negligible during high-temperature mantle melting and fractional crystallization (15), these correlations are best explained as mixing of melts derived from discrete mantle components with different $\delta^{11}\text{B}$ values. While B has a similar partition coefficient to Nb and Ce during mantle melting and melt fractionation, it is much more fluid mobile; therefore, elevated B/Nb and B/Ce ratios indicate fluid enrichment in the mantle source (15). B isotopic compositions and B/Nb and B/Ce ratios of the late-stage basalts correlate with Sr/Ce, K/U, and La/Yb ratios, and these correlations are consistent with melt mixing between a metasomatized SCLM and the local asthenosphere mantle (Figs. 2 and 3). While some of these correlations are not as strong for the early-stage basalts, likely because of stronger compositional similarities between the mantle end-members sampled by the early-stage basalts (e.g., Sr, Nd, and Zn isotopes; Fig. 4), the overall trends delineated by these two groups of basalts, and the excellent correlations between $\delta^{11}\text{B}$ and indices of depth or degree of melting (e.g., SiO_2 and La/Yb), support our hypothesis that the B isotopes in the studied samples reflect their mantle source signatures. Last, the early-stage basalts show higher overall B concentrations and higher B/Ce ratios at a given Sr/Ce ratio than the late-stage basalts (fig. S2 and Fig. 3), which indicate that they may come from a mantle source more enriched in B. However, the lower degrees of partial melting of

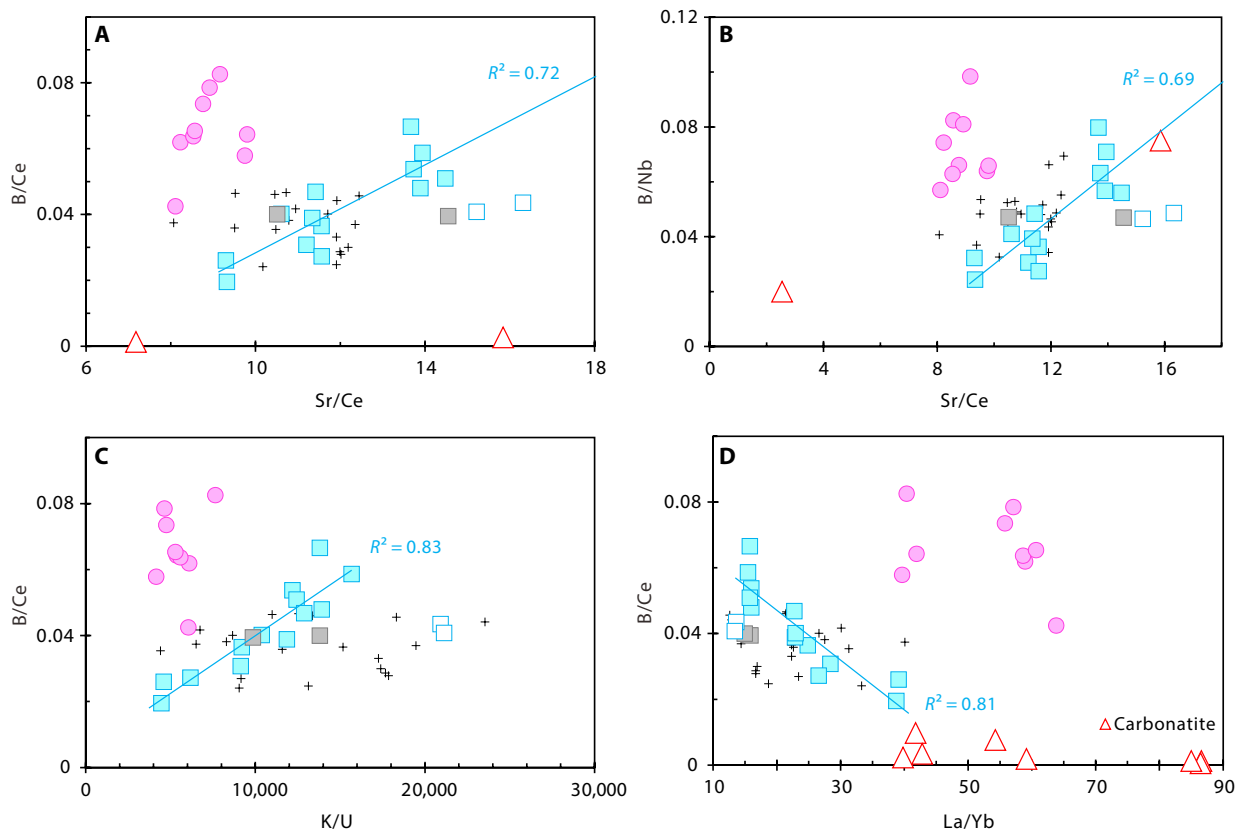


Fig. 3. B/Ce and B/Nb variation as a function of Sr/Ce, K/U, and La/Yb for the studied samples. (A) B/Ce versus Sr/Ce, (B) B/Nb versus Sr/Ce, (C) B/Ce versus K/U, and (D) B/Ce versus La/Yb. The best-fit regressions with R^2 values are shown. Symbols and regression lines follow Fig. 2. Data for carbonatites including both mantle and crustal origins are from (92).

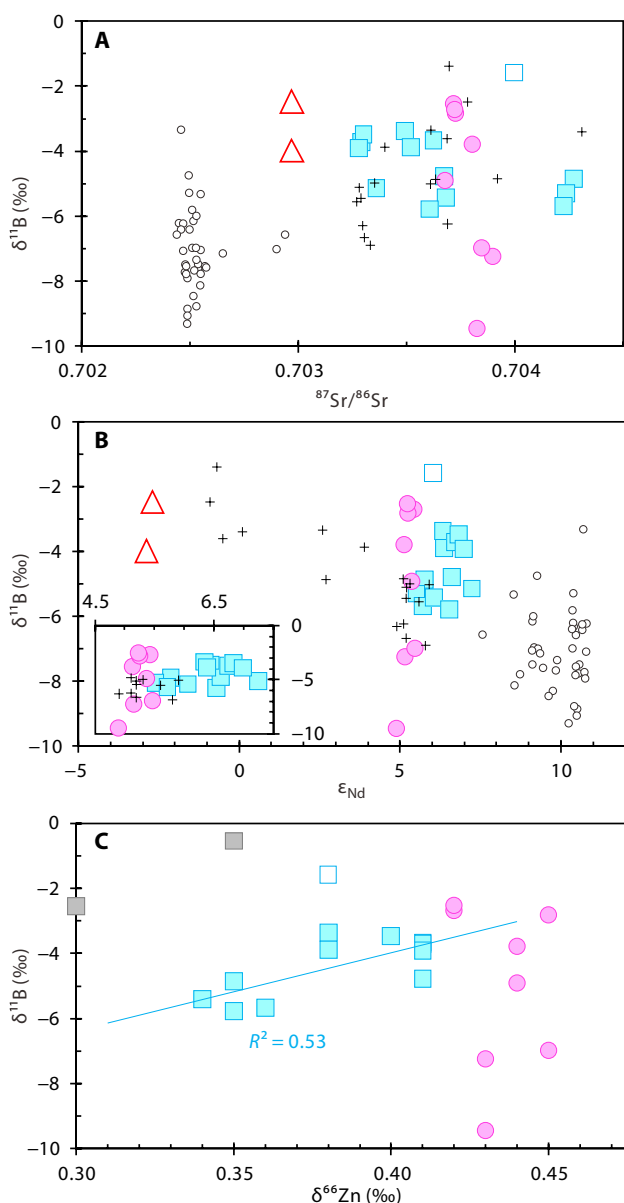


Fig. 4. Boron isotopes versus other isotopic tracers. $\delta^{11}\text{B}$ variation as a function of (A) $^{87}\text{Sr}/^{86}\text{Sr}$, (B) ϵ_{Nd} , and (C) $\delta^{66}\text{Zn}$ for the studied samples. Symbols and regression lines follow Fig. 2. The inset in (B) shows the enlargement of our data.

the early-stage basalts may also have contributed to their elevated B concentrations.

Recycled dehydrated slabs generated sub-MORB $\delta^{11}\text{B}$ in the early-stage basalts

The lowest $\delta^{11}\text{B}$ value (-9.5‰) among studied basalts is found in the early-stage lavas, which is distinctly lower than the proposed range for the depleted mantle ($\delta^{11}\text{B} = -7.1 \pm 0.9\text{‰}$) (15). In addition, most MORBs have B/Ce ratios greater than 0.09, while the studied basalts have B/Ce ratios between 0.02 and 0.08 (Fig. 2F) (15, 52). This observation indicates that a B-depleted mantle source with light $\delta^{11}\text{B}$ is required for the petrogenesis of basalts. The lightest B isotope ($\delta^{11}\text{B} = -9.5\text{‰}$) of our samples is similar to the lowest

$\delta^{11}\text{B}$ values reported for OIBs: -10.0‰ at Fogo (Cape Verde), -10.5‰ at La Palma (Canary), -10.8‰ at MacDonald Seamounts, and -10.6‰ at Holuhraun (Iceland) (Fig. 1), all of which have been attributed to the inclusion of dehydrated oceanic crust components in their mantle sources (35–37). This is because fluids released from the subducted slab preferentially concentrate heavy B isotopes, thereby generating residual slabs that are isotopically light and [B] depleted (21, 25, 26). Considered together with their elevated La/Yb ratios, the most likely candidate for the B-depleted and isotopically light component in the early-stage basalts is partial melts derived from a dehydrated recycled oceanic crust. In addition to B, slab dehydration should also efficiently squeeze out H_2O from the top portion of the slab, thereby generating low $\text{H}_2\text{O}/\text{Ce}$ ratios in the dehydrated slab residue. The early-stage basalts have lower $\text{H}_2\text{O}/\text{Ce}$ ratios (100 to 200) (43) than the depleted MORB mantle and MORBs (37, 72) but similar $\text{H}_2\text{O}/\text{Ce}$ ratios to HIMU basalts (72), which further support the presence of similar fluid-starved dehydrated oceanic crust components in their mantle sources.

Although melts from the dehydrated oceanic crust alone can account for most of the geochemical characteristics of the low- $\delta^{11}\text{B}$ end-member of the early-stage lavas, it cannot explain their slightly more enriched Sr and Nd isotopes and similar Ce/Pb ratio relative to MORBs (Figs. 2 and 4). The dehydrated oceanic crust should have higher Ce/Pb, because of the high mobility of Pb in fluids, and have Sr and Nd isotopes similar to the MORB protolith. The enriched Sr and Nd isotopes and relatively low Ce/Pb ratios of the low- $\delta^{11}\text{B}$ end-member are more consistent with the contribution of recycled siliceous sediments. Most subducting plates contain abundant siliceous sediments, including the present-day Pacific plate off the trench of Japan and Izu-Bonin Mariana (73). Siliceous sediments have high B contents (63 to 163 $\mu\text{g/g}$) and a wide range of $\delta^{11}\text{B}$ (-13.1 to 4.0‰) (23, 28), while subduction-related prograde metasediments have $\delta^{11}\text{B}$ values as low as -15‰ (74). Siliceous clays also contain abundant water, which should cause substantial B loss and B isotope fractionation during subduction, leading to relatively low $\delta^{11}\text{B}$ values in recycled siliceous sediments (75). While they are generally not considered a major source of B in the deep mantle because of their low volume and the extensive B loss at shallow levels, siliceous sediments have much higher Pb, Nd, and Sr contents and more enriched Sr and Nd isotopes than MORBs (73). As such, contributions from a small amount of recycled siliceous sediments along with the dehydrated oceanic crust could explain the observed slightly more enriched Sr and Nd isotopes, as well as the relatively low Ce/Pb ratios of the low- $\delta^{11}\text{B}$ end-member of the early-stage basalts.

Metasomatized SCLM as the low- $\delta^{11}\text{B}$ component in the late-stage basalts

Previous studies have established that a subduction-metasomatized SCLM component, with relatively elevated Si content, high Ba/Th, K/La, and Sr/Nd ratios, enriched Sr and Nd isotope ratios, and light Zn and Fe isotope ratios, contributed to the formation of the late-stage basalts (40, 41). Boron isotopes and concentrations provide additional insights into the nature of this SCLM component. The late-stage basalts with ratios of higher fluid-mobile to fluid-immobile elements (e.g., Sr/Ce, K/U, B/Ce, and B/Nb) (Figs. 2 and 3) and stronger SCLM signatures also have lower $\delta^{11}\text{B}$, which indicates that the SCLM component likely has low $\delta^{11}\text{B}$ as well. However, the lowest $\delta^{11}\text{B}$ value (-5.8‰) sampled by the late-stage basalts is slightly higher than that of the depleted mantle ($-7.1 \pm 0.9\text{‰}$) (15) and the

low- $\delta^{11}\text{B}$ end-member sampled by the early-stage basalts, which suggests that the dehydrated oceanic crust is unlikely the source. Metasomatism by slab-derived fluids could increase the $\delta^{11}\text{B}$ of the local SCLM. However, the studied samples have much lower B/Nb ratios (Fig. 3) than typical MORBs (i.e., 0.15 to 1.05) (15). Such low ratios typically indicate the derivation of melts from relatively fluid-starved sources, such as arc lavas associated with an unusually hot slab (21), postcollisional mafic lavas from the Armenian sector of the active Arabia-Eurasia collision zone (76), and postcollisional ultrapotassic lavas in southern Tibet (77). Sugden *et al.* (76), in particular, attributed low $\delta^{11}\text{B}$ values down to -5% and B/Nb ratios of 0.03 to 0.25 along with relatively enriched Sr and Nd isotopes in Armenian postcollisional lavas to melting of the lithospheric mantle that was metasomatized by Si-rich melts or fluids derived from subducted sediments. Meanwhile, without the inputs from the dehydrated oceanic crust, magmas from continental collision zones extend to much lower $\delta^{11}\text{B}$ than the depleted mantle (77). Given the elevated SiO_2 , enriched Nd and Sr isotopes, and low B/Ce and B/Nb but elevated Ce/Pb ratios of the late-stage basalts, we propose that the low- $\delta^{11}\text{B}$ mantle source of the late-stage basalts came from a SCLM that was mostly metasomatized by dehydrated subducted sediments. This hypothesis is supported by several lines of geochemical evidence. Sr, Nd, and Pb isotope compositions of mantle xenoliths in South China show EM2-type signatures, which were attributed to sediments added into the SCLM by the Mesozoic subduction of the paleo-Pacific plate (47, 78, 79). The SCLM-derived lavas from SE China have arc-like trace element signatures (e.g., enriched in large-ion lithophile elements and depleted in high-field-strength elements) and crustal-like enriched Sr and Nd isotope compositions, which suggest that the SCLM mantle source underneath South China might have received contributions from subducted sediments (80). Thermobarometry also suggests that the late-stage basalts originated from the lower part of the SCLM or within the lithosphere-asthenosphere boundary (40).

As mentioned earlier, two samples of the late-stage basalts have the highest $\delta^{11}\text{B}$ values among all the samples measured (white squares in Figs. 2 to 4). These two samples also have low B concentrations (fig. S2) and lower B/Ce and B/Nb ratios relative to the trend line defined by the late-stage basalts (Fig. 3). With these differences aside, their major and minor element contents and Sr, Nd, Fe, and Zn isotopic compositions fall along the trend defined by other late-stage basalts (fig. S1) (40, 41). These two samples are both from the Tiantai region, but they both show notably lower pressure of magma segregation (~ 2.5 GPa) than the other samples in the same area (3 to 3.8 GPa) (40). The SCLM beneath eastern China likely has a complex history involving multiple episodes of melt depletion and metasomatism, which could also lead to a range of boron concentration and isotopic compositions (81). Hence, we propose that these two samples record this variability by being equilibrated at a different pressure and sampling a SCLM component that was affected by a higher degree of metasomatism, resulting in higher K/La, Ba/Th, and Sr/Nd ratios (40).

Recycled carbonate as the common heavy boron end-member

One of the most notable features of our continental intraplate basalts is that in most cross plots, the two groups of samples converge toward a common component with $\delta^{11}\text{B}$ of about -2% (Figs. 2 and 4C). This component is unlikely to have been a hydrous fluid or

fluid-rich component like serpentinite because samples with high $\delta^{11}\text{B}$ show low B/Ce and Sr/Ce ratios and high Ce/Pb ratios (Fig. 2). On the basis of its low SiO_2 , Ti/Eu, Sr/Ce, and K/U and high La/Yb, La/Sm, Ce/Pb, Ca/Al, and $\delta^{66}\text{Zn}$ values (Figs. 2 to 4 and fig. S4), the most likely source for the common heavy $\delta^{11}\text{B}$ component is recycled carbonates. The primitive mantle-normalized trace element patterns of the early-stage low-silica samples closely resemble those of oceanic magnesio- and calcio-carbonatites (82), group I kimberlites, and high-Mg carbonate melts found in fluid inclusions within diamonds (83), MTZ-derived deep diamond inclusion (11-ON-ZIZ) with HIMU-like incompatible trace element patterns (84), and typical oceanic HIMU basalts (85) (fig. S5). Specifically, carbonate melts are distinguished by their low silica content, high CaO/ Al_2O_3 ratios, and elevated ratios of light to heavy rare-earth elements (e.g., La/Yb). They also exhibit pronounced depletion in high-field-strength elements (e.g., Zr, Hf, and Ti), as well as lower Pb and K contents relative to those of rare-earth elements (82). These depletions are attributed to the remarkably higher bulk partition coefficients of these elements compared to neighboring rare-earth elements in mantle rocks equilibrated with carbonate melts (86). Consequently, carbonate melts are typically characterized by low K/La, K/U, and Ti/Eu ratios, alongside high Ce/Pb and La/Yb ratios, which are also characteristics shown by our early-stage basalts. As such, the common high- $\delta^{11}\text{B}$ end-member could be related to recycled carbonates. Mg and Zn isotopes are supportive of this hypothesis (48, 87–89). Because isotopic fractionation of Zn and Mg during mantle partial melting is limited, and given the fact that recycled carbonates exhibit remarkably lighter Mg isotopes and heavier Zn isotopes compared to the normal mantle, the heavy Zn isotopes in our samples, along with the light Mg isotopes observed in similar samples from the same region reported in previous studies, suggest that recycled sedimentary carbonates played an important role in the formation of these lavas (40, 48, 51, 87–90). An involvement of recycled carbonates is also supported by the low B/Ce ratios (0.02 to 0.08) of the studied basalts, which fall between values of carbonatites associated with recycled crustal carbon (<0.01) (91, 92) and MORBs (~ 0.10) (15) (Fig. 2F). On the basis of evidence from multiple tracers, the B isotope and concentration data suggest that the heavy B mantle component sampled by the studied deeply sourced continental intraplate basalts could be recycled surface carbonate. If it is found to be true, then this is strong evidence that recycled carbonates can be preserved in the deep mantle, even in the MTZ.

To explain the low B/Ce but high $\delta^{11}\text{B}$ values of OIBs, Marshall *et al.* (38) called for a “rehydration” process where the low $\delta^{11}\text{B}$ value of the recycled devolatilized oceanic crust could be overprinted by fluids with high $\delta^{11}\text{B}$ values. Numerical modeling suggests that as temperature and pressure increase during subduction, the serpentinized lithospheric mantle underlying the devolatilized oceanic crust would dehydrate, generating fluids with high- δD and high- $\delta^{11}\text{B}$ signatures that can move upward and interact with the fluid-starved dehydrated oceanic crust without substantially increasing the B and H_2O budget of the slab (48–52). Further recycling of this rehydrated, devolatilized oceanic crust might therefore transfer a sub-MORB B/Ce ratio and high- $\delta^{11}\text{B}$ signature into the deep mantle. Such a serpentinite rehydration process has been previously called upon to explain heavy $\delta^{11}\text{B}$ values found in oceanic intraplate volcanism, even far from any subduction zones (fig. S3) (38, 93). Although intriguing, this type of rehydrated, devolatilized oceanic crust, with its high- $\delta^{11}\text{B}$ signature inherited from slab serpentinite,

is unlikely the source for the common heavy $\delta^{11}\text{B}$ component delineated by the studied basalts, as melt from this component should have high silica, Sr/Ce, and K/U, low Ce/Pb, and high $\delta^{26}\text{Mg}$ values. In particular, previous studies reported that the range of Mg isotope ratios for Cenozoic basalts in South China (including some basalts from the sampling sites of this study) spans from -0.60 to -0.28‰ (48, 68, 87, 88). These values are generally lower than the mantle baseline of $-0.25 \pm 0.07\text{‰}$ (94) and remarkably lower than the published Mg isotope data for serpentinites [with $\delta^{26}\text{Mg}$ values all exceeding -0.30‰ ; see figure S4 in (95)]. Collectively, these lines of evidence strongly argue against the substantial contribution of recycled serpentinites or rehydrated devolatilized oceanic crust to the mantle source of the studied samples.

So far, aside from a few studies of carbonatites that have presented evidence of recycled carbonates based on positive correlations between their $^{87}\text{Sr}/^{86}\text{Sr}$ and $\delta^{11}\text{B}$ (up to 5.5‰ , Fig. 1) (91, 92), to the best of our knowledge, no other studies of B isotopes have attributed heavy $\delta^{11}\text{B}$ found in intraplate basalts or even diamonds (96) to recycled carbonates. Marine carbonates have moderate B contents (13 to $26 \mu\text{g/g}$) and positive $\delta^{11}\text{B}$ values ($+4$ to $+33\text{‰}$) (Fig. 1) (28–32). It is generally assumed that even though carbonates do not contain a lot of water in their crystal lattice, interaction with slab-derived fluids should also drive off B and ^{11}B from carbonates during subduction. Our finding of the fluid-starved low-silica component with elevated $\delta^{66}\text{Zn}$ and $\delta^{11}\text{B}$ values in deeply sourced primitive intraplate basalts further supports the hypothesis that marine carbonates can preserve relatively heavy B isotopic signatures through the subduction process.

At subarc depths in subduction zones, dehydration of the subducting oceanic crust may lead to the dissolution and decarbonation of carbonates, releasing carbon into the mantle wedge that could be sampled by arc volcanism (97, 98). However, a small fraction of carbonates preserved in the subducting oceanic crust may not undergo decarbonation at these shallow depths. Instead, theoretical modeling (99) and experimental petrology (1, 100) suggested that as subduction progresses, they can be transported, in the form of carbonated eclogitic oceanic crust, into the deeper mantle, even reaching the MTZ. High-resolution geophysical tomography images have shown that the subducted Pacific slab is stalled and flattens at the lower part of the MTZ beneath the eastern margin of the Eurasian continent (Fig. 5) (46). Given that the distribution of voluminous alkaline mafic volcanism with strong carbonate signatures in eastern China is spatially coincident with the highly conductive electrical characteristics (101) and the geophysically observed low- P -wave seismic velocity anomalies (46) in the upper mantle above the MTZ, a genetic linkage between alkali basalts and the carbonated Pacific oceanic crust within the MTZ has been reasonably well established (47–49, 89). This volatile-rich MTZ (102–104), together with the stagnant slab, may serve as an important source and explain the occurrences of abundant enriched continental intraplate volcanism in eastern China (47, 48, 63, 64, 89, 105, 106). This is consistent with the hypothesis that during thermal equilibration with the ambient mantle over time, the nominal solidus of a carbonate-bearing subducted oceanic slab (carbonated MORB eclogite) may be crossed at a depth close to the MTZ, generating incipient alkaline carbonate melt with a low viscosity (100) that contributes to the genesis of intraplate alkali basalts.

Although subducting slabs lose a large amount of heavy ^{11}B during shallow dehydration, the subducted carbonated oceanic crust

can, however, remain stable up to the depth of the MTZ, as mentioned above, carrying small amounts of surface carbonate with a heavy B isotope signature into the MTZ. The relatively high $\delta^{11}\text{B}$ values in the continental intraplate basalts investigated in the present study provide geochemical evidence for crustal carbonate, most likely recycled together with the subduction of the Pacific plate, to survive the devolatilization process during subduction and be transported into the MTZ (Fig. 5). This hypothesis would also explain the anomalous Mg isotope compositions of silica-undersaturated continental intraplate basalts in eastern China that cannot be explained by melting of serpentinites or a decarbonated eclogite with metal isotope signatures inherited from carbonates in their protolith. Considered together with observations from geophysics and comprehensive geochemical evidence, our finding of a common mantle component for primitive continental intraplate basalts with signatures of recycled carbonates, heavy B isotopes, and low B/Ce ratios provides strong evidence that subducted carbonates play an important role in deep mantle melting (Fig. 5) and their influence on mantle chemistry may be even more pervasive than previously thought.

MATERIALS AND METHODS

Analytical methods

Boron abundances and isotope ratios were measured on a Neptune Plus MC-ICP-MS at Nanjing Institute of Geology and Palaeontology, Chinese Academy of Sciences (NIGPAS), following an alkaline fusion method outlined by Cai *et al.* (107). Briefly, 200 mg of sample powder was decomposed using hydrated Na_2O_2 in silver crucibles at 720°C in a muffle furnace. After cooling, the alkaline cake was dissolved with water and B was purified using Amberlite IRA-743 B-specific resin in an ISO class 5 Ultraclean chemistry laboratory with B-free polytetrafluoroethylene high-efficiency particulate air filters. B contents were determined on aliquots of the solution from the same dissolution through isotope dilution using a calibrated SRM 952 ^{10}B -enriched spike. B content and isotope compositions of international standards measured along with the samples, BCR-2, JB-2, and IAEA-B-5 all fall within published ranges (table S1).

Evaluating the effect of crustal contamination and low-temperature alteration

Crustal assimilation during magma emplacement and post-eruptive alteration are processes known to potentially affect the primary B isotope composition of the basaltic magmas [e.g., (108, 109)]; it is, therefore, essential to assess their possible influence on the B isotope composition of the studied basalts. In the suite of basalts from the Zhejiang area, two samples have been identified as having been affected by crustal contamination (18SZ18 and 18SZ19; i.e., gray squares in Figs. 2 and 3) (40). These two samples have the highest SiO_2 contents ($\sim 50 \text{ wt } \%$) of the suite, the lowest Nb/U and Ce/Pb ratios, and enriched Sr and Nd isotopic compositions than other samples from the same locality (fig. S6). These two samples also have low B concentrations (fig. S2) and heavy B isotope signatures (Figs. 2 and 3). Because of the large variations observed in the continental crust (-30 to $+22\text{‰}$) (108), a mean value for the crust is difficult to define. However, I-type granitic magmas are isotopically notably heavier ($\delta^{11}\text{B} = -2 \pm 5\text{‰}$) than S-type granitic rocks ($\delta^{11}\text{B} = -11 \pm 4\text{‰}$) (109). The latter corresponds to the commonly cited B isotope value of $\sim -10\text{‰}$ for the continental crust [e.g., (15, 109)]. Because much of Earth's crust is derived from I-type magmas, its

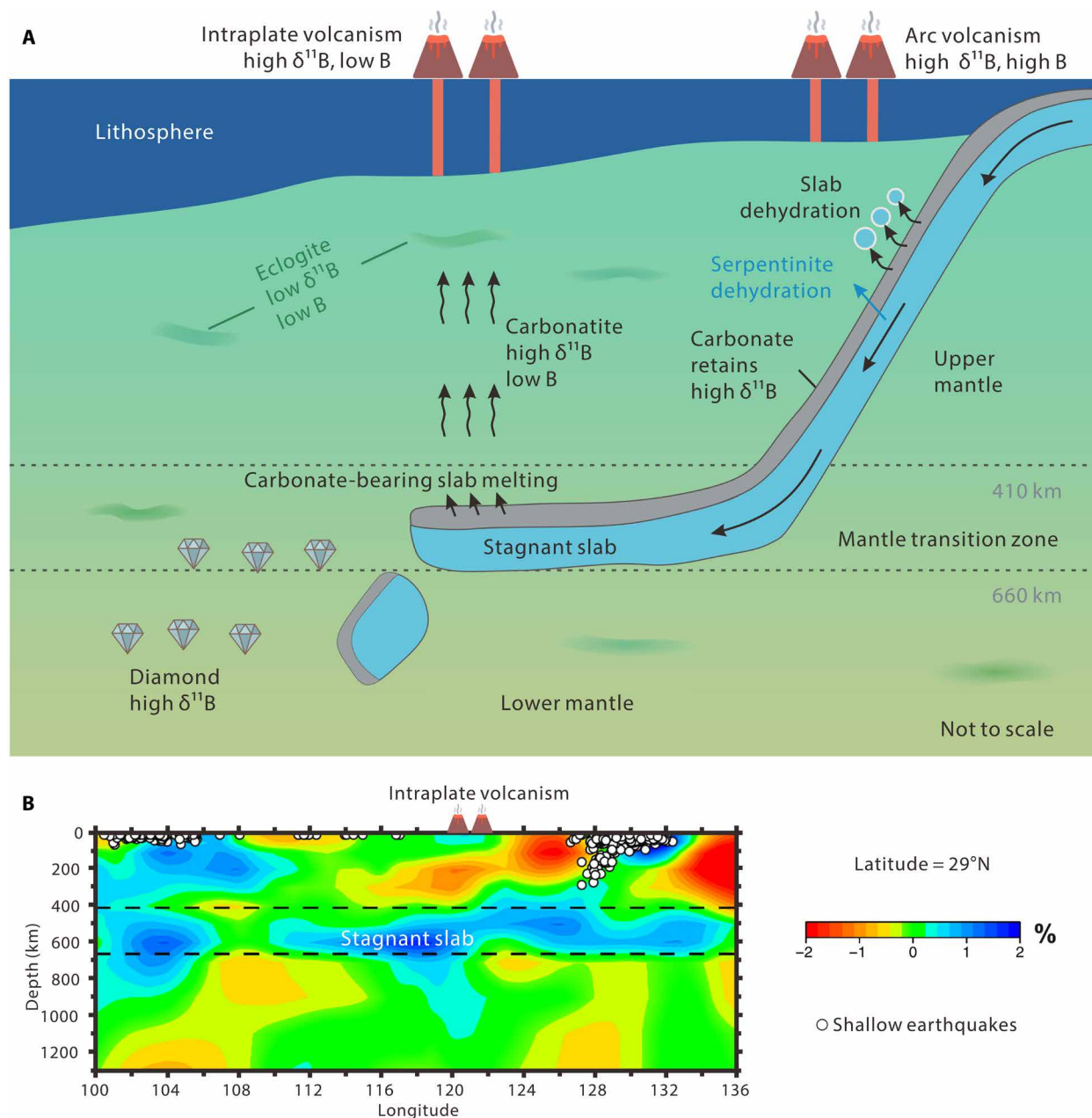


Fig. 5. Conceptual cartoon and geophysical tomography describing the generation of high- $\delta^{11}\text{B}$ intraplate magmas. (A) During plate subduction, dehydration of slab and its underlying lithospheric serpentinite at shallow depths less than 200 km supplies arc volcanism, while subducted carbonate-bearing slab carries heavy ^{11}B into the deep mantle, as revealed by high $\delta^{11}\text{B}$ values in intraplate magma and ultradeep diamonds. See text for details. **(B)** Vertical cross section of tomographic image of P -wave velocity anomalies at 29°N (46).

average B isotope value is probably higher. Here, we propose that the heavy B isotopic signatures observed for the samples 18SZ18 and 18SZ19 are consistent with crustal contamination. This is consistent with the low Nb/U ratios reported for these samples (fig. S6) and their low $^{143}\text{Nd}/^{144}\text{Nd}$ ratios (fig. S1).

Two other late-stage basalts (white squares in Figs. 2 to 4) also show heavier B isotopic compositions relative to the other late-stage basalts along with low B concentrations (fig. S2). These samples have elevated Nb/U ratios (fig. S6) and Sr-Nd isotopic compositions that fall along the trend of the late-stage basalts (fig. S1), which are

inconsistent with substantial impacts of crustal contamination. Their B/La (~ 0.08), B/Nb (~ 0.05), and B/Zr (0.12 to 0.13) ratios also fall within the range defined by the other late-stage basalts (0.04 to 0.13, 0.02 to 0.08, and 0.10 to 0.22, respectively, for the three ratios). As B is a highly mobile element, low-temperature alteration can affect B concentrations by preferentially leaching boron over immobile elements (e.g., La, Nb, and Zr). Hence, if the distinct B signature of these two samples was the result of alteration, they would also present distinct B/La, B/Nb, or B/Zr ratios, which are not observed here. In addition, because the heavier isotope (^{11}B) partitions more

readily into aqueous solution than the lighter isotope (^{10}B) (19), in the absence of seawater, low-temperature weathering of basalts should reduce their $\delta^{11}\text{B}$ value rather than increasing it. Hence, with no evidence for either crustal contamination or alteration, we propose that the B signatures of these samples are primary and, hence, we discuss the potential origin of these higher $\delta^{11}\text{B}$ values in the main text.

Supplementary Materials

This PDF file includes:

Figs. S1 to S6

Table S1

References

REFERENCES AND NOTES

- R. Dasgupta, M. M. Hirschmann, The deep carbon cycle and melting in Earth's interior. *Earth Planet. Sci. Lett.* **298**, 1–13 (2010).
- A. W. Hofmann, Mantle geochemistry: The message from oceanic volcanism. *Nature* **385**, 219–229 (1997).
- W. M. White, Oceanic island basalts and mantle plumes: The geochemical perspective. *Annu. Rev. Earth Planet. Sci.* **38**, 133–160 (2010).
- A. Zindler, S. Hart, Chemical geodynamics. *Annu. Rev. Earth Planet. Sci.* **14**, 493–571 (1986).
- A. Stracke, Earth's heterogeneous mantle: A product of convection-driven interaction between crust and mantle. *Chem. Geol.* **330**, 274–299 (2012).
- A. V. Sobolev, A. W. Hofmann, D. V. Kuzmin, G. M. Yaxley, N. T. Arndt, S. L. Chung, L. V. Danyushevsky, T. Elliott, F. A. Frey, M. O. Garcia, A. A. Gurenko, V. S. Kamenetsky, A. C. Kerr, N. A. Krivolutskaya, V. V. Matvienkov, I. K. Nikogosian, A. Rocholl, I. A. Sigurdsson, N. M. Sushchevskaya, M. Teklay, The amount of recycled crust in sources of mantle-derived melts. *Science* **316**, 412–417 (2007).
- Y. Niu, M. Wilson, E. R. Humphreys, M. J. O'Hara, The origin of intra-plate ocean island basalts (OIB): The lid effect and its geodynamic implications. *J. Petrol.* **52**, 1443–1468 (2011).
- R. Dasgupta, M. M. Hirschmann, Melting in the Earth's deep upper mantle caused by carbon dioxide. *Nature* **440**, 659–662 (2006).
- J. M. Brenan, E. B. Watson, Partitioning of trace elements between carbonate melt and clinopyroxene and olivine at mantle *P-T* conditions. *Geochim. Cosmochim. Acta* **55**, 2203–2214 (1991).
- J. M. Brenan, E. B. Watson, Partitioning of trace elements between olivine and aqueous fluids at high *P-T* conditions: Implications for the effect of fluid composition on trace-element transport. *Earth Planet. Sci. Lett.* **107**, 672–688 (1991).
- X.-J. Wang, L.-H. Chen, A. W. Hofmann, T. Hanyu, H. Kawabata, Y. Zhong, L.-W. Xie, J.-H. Shi, T. Miyazaki, Y. Hirahara, T. Takahashi, R. Senda, Q. Chang, B. S. Vaglarov, J.-I. Kimura, Recycled ancient ghost carbonate in the Pitcairn mantle plume. *Proc. Natl. Acad. Sci. U.S.A.* **115**, 8682–8687 (2018).
- Z. Wang, Z. Zhang, M. K. Reichow, W. Tian, W. Kong, B. Liu, Tracing decarbonated eclogite in the mantle sources of Tarim continental flood basalts using Zn isotopes. *Geol. Soc. Am. Bull.* **135**, 1768–1782 (2023).
- Q. Xie, Z. Zhang, S. F. Foley, C. Chen, Z. Cheng, Y. Wang, W. Kong, Y. Lv, M. Santosh, Q. Jin, Transition from tholeiitic to alkali basalts via interaction between decarbonated eclogite-derived melts and peridotite. *Chem. Geol.* **621**, 121354 (2023).
- S.-J. Wang, F.-Z. Teng, S.-G. Li, Tracing carbonate–silicate interaction during subduction using magnesium and oxygen isotopes. *Nat. Commun.* **5**, 5328 (2014).
- H. R. Marschall, V. D. Wanless, N. Shimizu, P. A. P. von Strandmann, T. Elliott, B. D. Monteleone, The boron and lithium isotopic composition of mid-ocean ridge basalts and the mantle. *Geochim. Cosmochim. Acta* **207**, 102–138 (2017).
- H.-Y. Li, X. Li, J. G. Ryan, C. Zhang, Y.-G. Xu, Boron isotopes in boninites document rapid changes in slab inputs during subduction initiation. *Nat. Commun.* **13**, 993 (2022).
- G. F. Cooper, C. G. Macpherson, J. D. Blundy, B. Maunder, R. W. Allen, S. Goes, J. S. Collier, L. Bie, N. Harmon, S. P. Hicks, A. A. Iveson, J. Prytulak, A. Rietbrock, C. A. Rychert, J. P. Davidson, the VoiLA team, Variable water input controls evolution of the Lesser Antilles volcanic arc. *Nature* **582**, 525–529 (2020).
- M. R. Palmer, G. H. Swihart, Boron isotope geochemistry: An overview. *Rev. Mineral. Geochem.* **33**, 709–744 (1996).
- R. L. Hervig, G. M. Moore, L. B. Williams, S. M. Peacock, J. R. Holloway, K. Roggensack, Isotopic and elemental partitioning of boron between hydrous fluid and silicate melt. *Am. Mineral.* **87**, 769–774 (2002).
- C. Schmidt, R. Thomas, W. Heinrich, Boron speciation in aqueous fluids at 22 to 600°C and 0.1 MPa to 2 GPa. *Geochim. Cosmochim. Acta* **69**, 275–281 (2005).
- W. P. Leeman, S. Tonarini, L. H. Chan, L. E. Borg, Boron and lithium isotopic variations in a hot subduction zone—The southern Washington Cascades. *Chem. Geol.* **212**, 101–124 (2004).
- M. Rosner, J. Erzinger, G. Franz, R. B. Trumbull, Slab-derived boron isotope signatures in arc volcanic rocks from the Central Andes and evidence for boron isotope fractionation during progressive slab dehydration. *Geochem. Geophys. Geosyst.* **4**, 9005 (2003).
- S. Tonarini, W. P. Leeman, P. T. Leat, Subduction erosion of forearc mantle wedge implicated in the genesis of the South Sandwich Island (SSI) arc: Evidence from boron isotope systematics. *Earth Planet. Sci. Lett.* **301**, 275–284 (2011).
- J. C. M. De Hoog, I. P. Savov, "Boron isotopes as a tracer of subduction zone processes" in *Boron Isotopes: The Fifth Element*, H. Marschall, G. Foster, Eds. (Springer, 2018), chap. 9, pp. 217–247.
- Y. Yu, X.-L. Huang, M. Sun, J.-L. Ma, B isotopic constraints on the role of H_2O in mantle wedge melting. *Geochim. Cosmochim. Acta* **303**, 92–109 (2021).
- P.-P. Liu, D.-B. Wang, M.-F. Zhou, X.-H. Li, Q.-L. Li, G. A. Gaetani, B. Monteleone, V. Kamenetsky, Constraints of boron and oxygen stable isotopes on dehydration fluids, sediment-derived melts, and crustal assimilation of the Toba volcanic system (Indonesia). *Geology* **52**, 161–165 (2023).
- D. Wang, R. L. Romer, J.-h. Guo, J. Glodny, Li and B isotopic fingerprint of Archean subduction. *Geochim. Cosmochim. Acta* **268**, 446–466 (2020).
- T. Ishikawa, E. Nakamura, Boron isotope systematics of marine sediments. *Earth Planet. Sci. Lett.* **117**, 567–580 (1993).
- N. G. Hemming, G. N. Hanson, Boron isotopic composition and concentration in modern marine carbonates. *Geochim. Cosmochim. Acta* **56**, 537–543 (1992).
- A. Vengosh, Y. Kolodny, A. Starinsky, A. R. Chivas, M. T. McCulloch, Coprecipitation and isotopic fractionation of boron in modern biogenic carbonates. *Geochim. Cosmochim. Acta* **55**, 2901–2910 (1991).
- S. Zhang, M. J. Henehan, P. M. Hull, R. P. Reid, D. S. Hardisty, A. v. S. Hood, N. J. Planavsky, Investigating controls on boron isotope ratios in shallow marine carbonates. *Earth Planet. Sci. Lett.* **458**, 380–393 (2017).
- Y. Zhang, C. Yuan, M. Sun, J. Li, X. Long, Y. Jiang, Z. Huang, Molybdenum and boron isotopic evidence for carbon-recycling via carbonate dissolution in subduction zones. *Geochim. Cosmochim. Acta* **278**, 340–352 (2020).
- X.-Y. Zhang, L.-H. Chen, X.-J. Wang, T. Hanyu, A. W. Hofmann, T. Komiya, K. Nakamura, Y. Kato, G. Zeng, W.-X. Gou, W.-Q. Li, Zinc isotopic evidence for recycled carbonate in the deep mantle. *Nat. Commun.* **13**, 6085 (2022).
- A. J. Spivack, J. M. Edmond, Boron isotope exchange between seawater and the oceanic crust. *Geochim. Cosmochim. Acta* **51**, 1033–1043 (1987).
- M. E. Hartley, J. C. M. de Hoog, O. Shorttle, Boron isotopic signatures of melt inclusions from North Iceland reveal recycled material in the Icelandic mantle source. *Geochim. Cosmochim. Acta* **294**, 273–294 (2021).
- K. J. Walowski, L. A. Kirstein, J. C. M. De Hoog, T. Elliott, I. P. Savov, R. E. Jones, EIMF, Boron recycling in the mantle: Evidence from a global comparison of ocean island basalts. *Geochim. Cosmochim. Acta* **302**, 83–100 (2021).
- K. J. Walowski, L. A. Kirstein, J. C. M. De Hoog, T. Elliott, I. P. Savov, R. E. Jones, Investigating ocean island mantle source heterogeneity with boron isotopes in melt inclusions. *Earth Planet. Sci. Lett.* **508**, 97–108 (2019).
- E. W. Marshall, E. Ranta, S. A. Halldórsson, A. Caracciolo, E. Bali, H. Jeon, M. J. Whitehouse, J. D. Barnes, A. Stefánsson, Boron isotope evidence for devolatilized and rehydrated recycled materials in the Icelandic mantle source. *Earth Planet. Sci. Lett.* **577**, 117229 (2022).
- J. Aggarwal, M. Palmer, T. D. Bullen, S. Arnórsson, K. Ragnarsdóttir, The boron isotope systematics of Icelandic geothermal waters: 1. Meteoric water charged systems. *Geochim. Cosmochim. Acta* **64**, 579–585 (2000).
- R. Xu, Y. Liu, S. Lambert, K. Hoernle, Y. Zhu, Z. Zou, J. Zhang, Z. Wang, M. Li, F. Moynier, K. Zong, H. Chen, Z. Hu, Decoupled Zn–Sr–Nd isotopic composition of continental intraplate basalts caused by two-stage melting process. *Geochim. Cosmochim. Acta* **326**, 234–252 (2022).
- R. Xu, S. Lambert, O. Nebel, M. Li, Z. Bai, J. Zhang, G. Zhang, J. Gao, H. Zhong, Y. Liu, Iron isotope evidence in continental intraplate basalts for mantle lithosphere imprint on heterogeneous asthenospheric melts. *Earth Planet. Sci. Lett.* **625**, 118499 (2024).
- K. Ho, J. Chen, C. Lo, H. Zhao, ^{40}Ar – ^{39}Ar dating and geochemical characteristics of late Cenozoic basaltic rocks from the Zhejiang–Fujian region, SE China: Eruption ages, magma evolution and petrogenesis. *Chem. Geol.* **197**, 287–318 (2003).
- S.-C. Liu, Q.-K. Xia, S. H. Choi, E. Deloule, P. Li, J. Liu, Continuous supply of recycled Pacific oceanic materials in the source of Cenozoic basalts in SE China: The Zhejiang case. *Contrib. Mineral. Petrol.* **171**, 100 (2016).
- Y.-Q. Li, C.-Q. Ma, P. T. Robinson, Q. Zhou, M.-L. Liu, Recycling of oceanic crust from a stagnant slab in the mantle transition zone: Evidence from Cenozoic continental basalts in Zhejiang Province, SE China. *Lithos* **230**, 146–165 (2015).

45. X. Yu, L.-H. Chen, G. Zeng, Growing magma chambers control the distribution of small-scale flood basalts. *Sci. Rep.* **5**, 16824 (2015).
46. J. Huang, D. Zhao, High-resolution mantle tomography of China and surrounding regions. *J. Geophys. Res.* **111**, B09305 (2006).
47. Y. Xu, H. Li, L. Hong, L. Ma, Q. Ma, M. Sun, Generation of Cenozoic intraplate basalts in the big mantle wedge under eastern Asia. *Sci. China Earth Sci.* **61**, 869–886 (2018).
48. S.-G. Li, W. Yang, S. Ke, X. Meng, H. Tian, L. Xu, Y. He, J. Huang, X.-C. Wang, Q. Xia, W. Sun, X. Yang, Z.-Y. Ren, H. Wei, Y. Liu, F. Meng, J. Yan, Deep carbon cycles constrained by a large-scale mantle Mg isotope anomaly in eastern China. *Nat. Sci. Rev.* **4**, 111–120 (2017).
49. R. Xu, Y. Liu, X.-C. Wang, S. F. Foley, Y. Zhang, H. Yuan, Generation of continental intraplate alkali basalts and implications for deep carbon cycle. *Earth Sci. Rev.* **201**, 103073 (2020).
50. G. Zeng, L.-H. Chen, A. W. Hofmann, X.-J. Wang, J.-Q. Liu, X. Yu, L.-W. Xie, Nephelinites in eastern China originating from the mantle transition zone. *Chem. Geol.* **576**, 120276 (2021).
51. X.-H. Dong, S.-J. Wang, W. Wang, S. Huang, Q.-L. Li, C. Liu, T. Gao, S. Li, S. Wu, Highly oxidized intraplate basalts and deep carbon storage. *Sci. Adv.* **10**, eadm8138 (2024).
52. A. Gale, C. A. Dalton, C. H. Langmuir, Y. Su, J.-G. Schilling, The mean composition of ocean ridge basalts. *Geochem. Geophys. Geosyst.* **14**, 489–518 (2013).
53. J. Liu, Z.-Z. Wang, H.-R. Yu, Q.-K. Xia, E. Delouie, M. Feng, Dynamic contribution of recycled components from the subducted Pacific slab: Oxygen isotopic composition of the basalts from 106 Ma to 60 Ma in North China Craton. *J. Geophys. Res. Solid Earth* **122**, 988–1006 (2017).
54. Y.-G. Xu, H.-H. Zhang, H.-N. Qiu, W.-C. Ge, F.-Y. Wu, Oceanic crust components in continental basalts from Shuangliao, Northeast China: Derived from the mantle transition zone? *Chem. Geol.* **328**, 168–184 (2012).
55. H.-Y. Li, Y.-G. Xu, J. G. Ryan, X.-L. Huang, Z.-Y. Ren, H. Guo, Z.-G. Ning, Olivine and melt inclusion chemical constraints on the source of intracratonic basalts from the eastern North China Craton: Discrimination of contributions from the subducted Pacific slab. *Geochim. Cosmochim. Acta* **178**, 1–19 (2016).
56. R. Xu, Y. Liu, X. Wang, K. Zong, Z. Hu, H. Chen, L. Zhou, Crust recycling induced compositional-temporal-spatial variations of Cenozoic basalts in the Trans-North China Orogen. *Lithos* **274**, 383–396 (2017).
57. W. Fang, L.-Q. Dai, Y.-F. Zheng, Z.-F. Zhao, Molybdenum isotopes in mafic igneous rocks record slabmantle interactions from subarc to postarc depths. *Geology* **51**, 3–7 (2023).
58. J.-Q. Liu, Z.-Y. Ren, A. R. L. Nichols, M.-S. Song, S.-P. Qian, Y. Zhang, P.-P. Zhao, Petrogenesis of Late Cenozoic basalts from North Hainan Island: Constraints from melt inclusions and their host olivines. *Geochim. Cosmochim. Acta* **152**, 89–121 (2015).
59. J. Liu, Q.-K. Xia, E. Delouie, H. Chen, M. Feng, Recycled oceanic crust and marine sediment in the source of alkali basalts in Shandong, eastern China: Evidence from magma water content and oxygen isotopes. *J. Geophys. Res. Solid Earth* **120**, 8281–8303 (2015).
60. J. Liu, Q.-K. Xia, E. Delouie, J. Ingrin, H. Chen, M. Feng, Water content and oxygen isotopic composition of alkali basalts from the Taihang Mountains, China: Recycled oceanic components in the mantle source. *J. Petrol.* **56**, 681–702 (2015).
61. Z. Zou, Z. Wang, S. Foley, R. Xu, X. Geng, Y.-N. Liu, Y. Liu, Z. Hu, Origin of low-MgO primitive intraplate alkaline basalts from partial melting of carbonate-bearing eclogite sources. *Geochim. Cosmochim. Acta* **324**, 240–261 (2022).
62. H.-K. Dai, J.-P. Zheng, S. Y. O'Reilly, W. L. Griffin, Q. Xiong, R. Xu, Y.-P. Su, X.-Q. Ping, F.-K. Chen, Langshan basalts record recycled Paleo-Asian oceanic materials beneath the northwest North China Craton. *Chem. Geol.* **524**, 88–103 (2019).
63. T. Sakuyama, W. Tian, J.-I. Kimura, Y. Fukao, Y. Hirahara, T. Takahashi, R. Senda, Q. Chang, T. Miyazaki, M. Obayashi, H. Kawabata, Y. Tatsumi, Melting of dehydrated oceanic crust from the stagnant slab and of the hydrated mantle transition zone: Constraints from Cenozoic alkaline basalts in eastern China. *Chem. Geol.* **359**, 32–48 (2013).
64. H. Chen, Q.-K. Xia, J. Ingrin, E. Delouie, Y. Bi, Heterogeneous source components of intraplate basalts from NE China induced by the ongoing Pacific slab subduction. *Earth Planet. Sci. Lett.* **459**, 208–220 (2017).
65. S.-P. Qian, Z.-Y. Ren, L. Zhang, L.-B. Hong, J.-Q. Liu, Chemical and Pb isotope composition of olivine-hosted melt inclusions from the Hannuoba basalts, North China Craton: Implications for petrogenesis and mantle source. *Chem. Geol.* **401**, 111–125 (2015).
66. G. Zeng, L.-H. Chen, X. Yu, J.-Q. Liu, X.-S. Xu, S. Erdmann, Magma-magma interaction in the mantle beneath eastern China. *J. Geophys. Res. Solid Earth* **122**, 2763–2779 (2017).
67. S.-Y. Yu, Y.-G. Xu, K.-J. Huang, J.-B. Lan, L.-M. Chen, S.-H. Zhou, Magnesium isotope constraints on contributions of recycled oceanic crust and lithospheric mantle to generation of intraplate basalts in a big mantle wedge. *Lithos* **398–399**, 106327 (2021).
68. X. Yu, G. Zeng, L.-H. Chen, X.-J. Wang, J.-Q. Liu, L.-W. Xie, T. Yang, Evidence for rutile-bearing eclogite in the mantle sources of the Cenozoic Zhejiang basalts, eastern China. *Lithos* **324–325**, 152–164 (2019).
69. H.-L. Zhang, G. Zeng, J.-Q. Liu, L.-H. Chen, J.-H. Yu, B. Wu, X.-J. Wang, X.-S. Xu, X.-W. Liu, Carbonated eclogitic component beneath eastern China revealed by olivine phenocrysts in nephelinites. *Chem. Geol.* **640**, 121744 (2023).
70. Z. Wei, H. Y. Li, L. Ma, Y.-S. Hou, Y. Wang, Y.-G. Xu, Geochemistry of olivine melt inclusion reveals interactions between deeply derived carbonated melts from the big mantle Wedge and Pyroxenite in the lithospheric mantle beneath Eastern Asia. *Geophys. Res. Lett.* **51**, e2024GL108234 (2024).
71. F.-B. Pan, C. Jin, X. He, L. Tao, B.-J. Jia, A plate-mantle convection system in the West Pacific revealed by tertiary ultramafic-mafic volcanic rocks in Southeast China. *Earth Space Sci.* **8**, e2020EA001324 (2021).
72. J. E. Dixon, L. Leist, C. Langmuir, J.-G. Schilling, Recycled dehydrated lithosphere observed in plume-influenced mid-ocean-ridge basalt. *Nature* **420**, 385–389 (2002).
73. T. Plank, "The chemical composition of subducting sediments" in *Treatise on Geochemistry*, H. D. Holland, K. K. Turekian, Eds. (Elsevier, 2014), vol. 4, pp. 607–629.
74. G. E. Bebout, E. Nakamura, Record in metamorphic tourmalines of subduction-zone devolatilization and boron cycling. *Geology* **31**, 407–410 (2003).
75. D. M. Saffer, A. J. Kopf, Boron desorption and fractionation in Subduction Zone Fore Arcs: Implications for the sources and transport of deep fluids. *Geochem. Geophys. Geosyst.* **17**, 4992–5008 (2016).
76. P. J. Suggden, I. P. Savov, S. Agostini, M. Wilson, R. Halama, K. Meliksetian, Boron isotope insights into the origin of subduction signatures in continent-continent collision zone volcanism. *Earth Planet. Sci. Lett.* **538**, 116207 (2020).
77. L.-L. Hao, Q. Wang, A. C. Kerr, G.-J. Wei, F. Huang, M.-Y. Zhang, Y. Qi, L. Ma, X.-F. Chen, Y.-N. Yang, Contribution of continental subduction to very light B isotope signatures in post-collisional magmas: Evidence from southern Tibetan ultrapotassic rocks. *Earth Planet. Sci. Lett.* **584**, 117508 (2022).
78. M. Tatsumoto, A. R. Basu, H. Wankang, W. Junwen, X. Guanghong, Sr, Nd, and Pb isotopes of ultramafic xenoliths in volcanic rocks of Eastern China: Enriched components EMI and EMII in subcontinental lithosphere. *Earth Planet. Sci. Lett.* **113**, 107–128 (1992).
79. H. Zou, A. Zindler, X. Xu, Q. Qi, Major, trace element, and Nd, Sr and Pb isotope studies of Cenozoic basalts in SE China: Mantle sources, regional variations, and tectonic significance. *Chem. Geol.* **171**, 33–47 (2000).
80. F. Guo, Y. Wu, B. Zhang, X. Zhang, L. Zhao, J. Liao, Magmatic responses to Cretaceous subduction and tearing of the paleo-Pacific Plate in SE China: An overview. *Earth Sci. Rev.* **212**, 103448 (2021).
81. M. R. Guild, "Boron isotopic composition of the subcontinental lithospheric mantle," thesis, Arizona State University (2014).
82. K. Hoernle, G. Tilton, M. J. Le Bas, S. Duggen, D. Garbe-Schönberg, Geochemistry of oceanic carbonatites compared with continental carbonatites: Mantle recycling of oceanic crustal carbonate. *Contrib. Mineral. Petrol.* **142**, 520–542 (2002).
83. Y. Weiss, W. L. Griffin, D. R. Bell, O. Navon, High-Mg carbonatitic melts in diamonds, kimberlites and the sub-continental lithosphere. *Earth Planet. Sci. Lett.* **309**, 337–347 (2011).
84. S. Huang, O. Tschauner, S. Yang, M. Humayun, W. Liu, S. N. Gilbert Corder, H. A. Bechtel, J. Tischler, HIMU geochemical signature originating from the transition zone. *Earth Planet. Sci. Lett.* **542**, 116323 (2020).
85. S. E. Mazza, E. Gazel, M. Bizimis, R. Moucha, P. Béguelin, E. A. Johnson, R. J. McAleer, A. V. Sobolev, Sampling the volatile-rich transition zone beneath Bermuda. *Nature* **569**, 398–403 (2019).
86. R. Dasgupta, M. M. Hirschmann, W. F. McDonough, M. Spiegelman, A. C. Withers, Trace element partitioning between garnet lherzolite and carbonatite at 6.6 and 8.6 GPa with applications to the geochemistry of the mantle and of mantle-derived melts. *Chem. Geol.* **262**, 57–77 (2009).
87. J. Huang, S.-G. Li, Y. Xiao, S. Ke, W.-Y. Li, Y. Tian, Origin of low $\delta^{26}\text{Mg}$ Cenozoic basalts from South China Block and their geodynamic implications. *Geochim. Cosmochim. Acta* **164**, 298–317 (2015).
88. Q.-Z. Jin, J. Huang, S.-C. Liu, F. Huang, Magnesium and zinc isotope evidence for recycled sediments and oceanic crust in the mantle sources of continental basalts from eastern China. *Lithos* **370–371**, 105627 (2020).
89. S.-A. Liu, Z.-Z. Wang, S.-G. Li, J. Huang, W. Yang, Zinc isotope evidence for a large-scale carbonated mantle beneath eastern China. *Earth Planet. Sci. Lett.* **444**, 169–178 (2016).
90. H. Beunon, N. Mattioli, L. S. Doucet, B. Moine, B. Debret, Mantle heterogeneity through Zn systematics in oceanic basalts: Evidence for a deep carbon cycling. *Earth Sci. Rev.* **205**, 103174 (2020).
91. S. R. W. Hulett, A. Simonetti, E. T. Rasbury, N. G. Hemming, Recycling of subducted crustal components into carbonatite melts revealed by boron isotopes. *Nat. Geosci.* **9**, 904–908 (2016).
92. O. Çimen, C. Kuebler, S. S. Simonetti, L. Corcoran, R. Mitchell, A. Simonetti, Combined boron, radiogenic (Nd, Pb, Sr), stable (C, O) isotopic and geochemical investigations of carbonatites from the Blue River Region, British Columbia (Canada): Implications for mantle sources and recycling of crustal carbon. *Chem. Geol.* **529**, 119240 (2019).
93. J. E. Dixon, I. N. Bindeman, R. H. Kingsley, K. K. Simons, P. J. Le Roux, T. R. Hajewski, P. Swart, C. H. Langmuir, J. G. Ryan, K. J. Walowski, I. Wada, P. J. Wallace, Light stable isotopic compositions of enriched mantle sources: Resolving the dehydration paradox. *Geochem. Geophys. Geosyst.* **18**, 3801–3839 (2017).
94. F.-Z. Teng, W.-Y. Li, S. Ke, B. Marty, N. Dauphas, S. Huang, F.-Y. Wu, A. Pourmand, Magnesium isotopic composition of the Earth and chondrites. *Geochim. Cosmochim. Acta* **74**, 4150–4166 (2010).

95. X.-Y. Qiao, J.-W. Xiong, Y.-X. Chen, J. C. De Hoog, J. Pearce, F. Huang, Z.-F. Zhao, K. Chen, Magnesium and boron isotope evidence for the generation of arc magma through serpentinite mélange melting. *Nat. Sci. Rev.* **12**, nwae363 (2025).
96. M. E. Regier, K. V. Smit, T. B. Chalk, T. Stachel, R. A. Stern, E. M. Smith, G. L. Foster, Y. Bussweiler, C. DeBuhr, A. D. Burnham, J. W. Harris, D. G. Pearson, Boron isotopes in blue diamond record seawater-derived fluids in the lower mantle. *Earth Planet. Sci. Lett.* **602**, 117923 (2023).
97. P. B. Kelemen, C. E. Manning, Reevaluating carbon fluxes in subduction zones, what goes down, mostly comes up. *Proc. Natl. Acad. Sci. U.S.A.* **112**, E3997–E4006 (2015).
98. T. Plank, C. E. Manning, Subducting carbon. *Nature* **574**, 343–352 (2019).
99. N. Coltice, L. Simon, C. Lécuyer, Carbon isotope cycle and mantle structure. *Geophys. Res. Lett.* **31**, L05603 (2004).
100. A. R. Thomson, M. J. Walter, S. C. Kohn, R. A. Brooker, Slab melting as a barrier to deep carbon subduction. *Nature* **529**, 76–79 (2016).
101. M. Ichiki, K. Baba, M. Obayashi, H. Utada, Water content and geotherm in the upper mantle above the stagnant slab: Interpretation of electrical conductivity and seismic P-wave velocity models. *Phys. Earth Planet. Inter.* **155**, 1–15 (2006).
102. Q.-K. Xia, J. Liu, I. Kovács, Y.-T. Hao, P. Li, X.-Z. Yang, H. Chen, Y.-M. Sheng, Water in the upper mantle and deep crust of eastern China: Concentration, distribution and implications. *Nat. Sci. Rev.* **6**, 125–144 (2019).
103. X.-C. Wang, S. A. Wilde, Q.-L. Li, Y.-N. Yang, Continental flood basalts derived from the hydrous mantle transition zone. *Nat. Commun.* **6**, 7700 (2015).
104. T. Kuritani, E. Ohtani, J.-I. Kimura, Intensive hydration of the mantle transition zone beneath China caused by ancient slab stagnation. *Nat. Geosci.* **4**, 713–716 (2011).
105. K.-C. Xing, F. Wang, F.-Z. Teng, W.-L. Xu, Y.-N. Wang, D.-B. Yang, H.-L. Li, Y.-C. Wang, Potassium isotopic evidence for recycling of surface water into the mantle transition zone. *Nat. Geosci.* **17**, 579–585 (2024).
106. J. Yang, M. Faccenda, Intraplate volcanism originating from upwelling hydrous mantle transition zone. *Nature* **579**, 88–91 (2020).
107. Y. Cai, T. Ruan, Y. Li, B. Li, W. Zhang, Z. Li, H. Wei, E. T. Rasbury, Improved alkaline fusion method for B isotope and concentration measurements of silicate materials. *J. Anal. At. Spectrom.* **38**, 1934–1942 (2023).
108. M. Chaussidon, F. Albarède, Secular boron isotope variations in the continental crust: An ion microprobe study. *Earth Planet. Sci. Lett.* **108**, 229–241 (1992).
109. R. B. Trumbull, J. F. Slack, "Boron isotopes in the continental crust: granites, pegmatites, felsic volcanic rocks, and related ore deposits" in *Boron Isotopes: The Fifth Element*, H. Marschall, G. Foster, Eds. (Springer, 2018), chap. 10, pp. 249–272.
110. R. Tanaka, E. Nakamura, Boron isotopic constraints on the source of Hawaiian shield lavas. *Geochim. Cosmochim. Acta* **69**, 3385–3399 (2005).
111. J. Liu, C. Tao, J. Zhou, K. Shimizu, W. Li, J. Liang, S. Liao, T. Kuritani, E. Delouie, T. Ushikubo, M. Nakagawa, W. Yang, G. Zhang, Y. Liu, C. Zhu, H. Sun, J. Zhou, Water enrichment in the mid-ocean ridge by recycling of mantle wedge residue. *Earth Planet. Sci. Lett.* **584**, 117455 (2022).
112. H.-Y. Li, Z. Zhou, J. G. Ryan, G.-J. Wei, Y.-G. Xu, Boron isotopes reveal multiple metasomatic events in the mantle beneath the eastern North China Craton. *Geochim. Cosmochim. Acta* **194**, 77–90 (2016).
113. H. R. Marschall, R. Altherr, L. Rüpke, Squeezing out the slab — Modelling the release of Li, Be and B during progressive high-pressure metamorphism. *Chem. Geol.* **239**, 323–335 (2007).
114. W. F. McDonough, S.-s. Sun, The composition of the Earth. *Chem. Geol.* **120**, 223–253 (1995).
115. R. L. Rudnick, S. Gao, "Composition of the continental crust" in *Treatise on Geochemistry*, H. D. Holland, K. K. Turekian, Eds. (Elsevier, 2003), vol. 3, pp. 1–64.
116. G. Zhu, J. Ma, G. Wei, L. Zhang, Boron mass fractions and $\delta^{11}\text{B}$ values of eighteen international geological reference materials. *Geostand. Geoanalytical Res.* **45**, 583–598 (2021).

Acknowledgments: We appreciate the reviewers as well as the editor for constructive comments. We are grateful to Y. Li and W.W. Zhang for assistance with boron isotope analysis, to S.-J. Wang and X.-H. Dong for sharing their compiled trace element data, and to Y. Chen and Z. Chen for providing information about the Mg isotope of serpentinite. We also thank E. T. Rasbury and W. Hu for helpful suggestions. **Funding:** This study was supported by the National Natural Science Foundation of China (42121003, 42122024, and 42472162), Key R&D Program of China (2019YFA0708400 and 2023YFF0804403), Strategic Priority Research Program of Chinese Academy of Sciences (XDA0430201), CAS "Light of West China" Program (xbzgzdsys-202310), Guizhou Provincial High Level Innovation Talent program (GCC [2023] 057), and Guizhou Provincial 2021 Science and Technology Subsidies (no. GZ2021SIG). **Author contributions:** R.X. designed the study and wrote the original draft. Y.C. performed analytical measurements and wrote the original draft. R.X., Y.C., and S.L. interpreted the data. All authors contributed to revising the manuscript. **Competing interests:** The authors declare that they have no competing interests. **Data and materials availability:** All data needed to evaluate the conclusions are present in the paper and/or the Supplementary Materials.

Submitted 21 August 2024

Accepted 18 March 2025

Published 23 April 2025

10.1126/sciadv.ads5104

Supplementary Materials for
**Heavy boron isotopes in intraplate basalts reveal recycled carbonate in
the mantle**

Rong Xu *et al.*

Corresponding author: Rong Xu, xurong@mail.gyig.ac.cn; Yue Cai, merrycai@gmail.com

Sci. Adv. **11**, eads5104 (2025)
DOI: 10.1126/sciadv.ads5104

This PDF file includes:

Figs. S1 to S6
Table S1
References

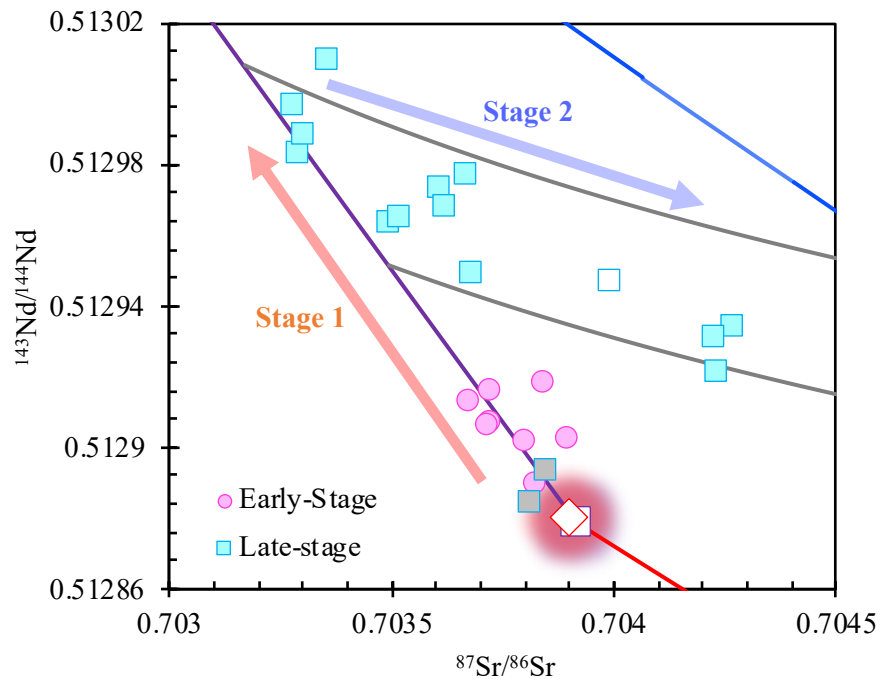


Figure S1. Sr-Nd isotope composition of the studied samples. Early-stage basalts are represented by the circles, late-stage basalts are represented by the squares, with the two grey squares being the samples affected by crustal contamination and the two open square being the samples that reflect boron heterogeneity of the SCLM (see discussion in text for details). The red line illustrates mixing between MORB-like eclogite and carbonate components to form the carbonated eclogite component. The purple curve represents the mixing line between DMM and carbonated eclogite component. The blue line represents mixing between the lithospheric mantle and GLOSS components and the gray lines illustrate the mixing range between the asthenospheric components and the subduction modified lithospheric component. See also Figure. 4 and Figure. S9 in ref (40) for details. The stage 1 arrow indicates decompression melting of the heterogeneous asthenosphere that dilutes the enriched signature of carbonated pyroxenite. The stage 2 arrow indicates mixing of melt from subduction-modified SCLM with the hybrid asthenospheric melt. See details in refs (40, 41).

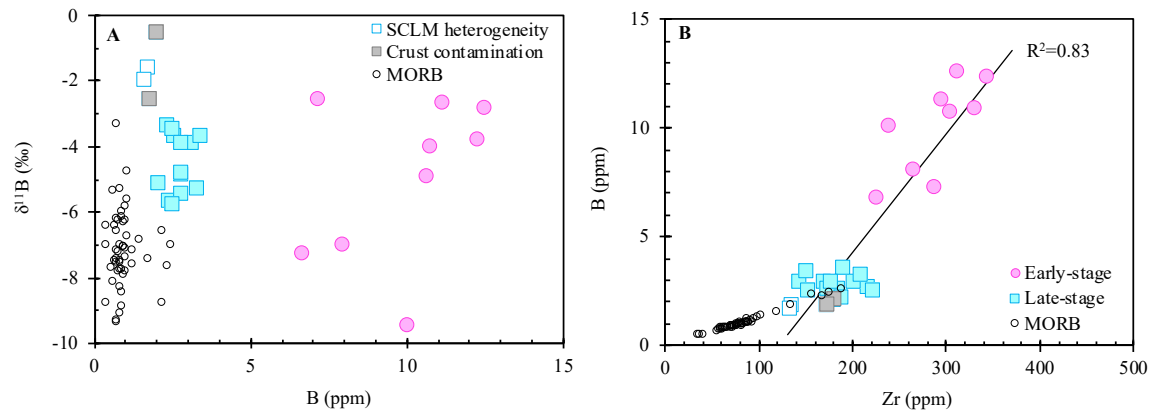


Fig. S2. (A) $\delta^{11}\text{B}$ versus B content and (B) B vs. Zr content of the studied samples. Symbols are as in Fig. 2 of main text. For the late-stage samples, four samples with heaviest B are shown in open and grey squares, with the two grey squares being the samples affected by crustal contamination and the two open squares being the samples that reflect boron heterogeneity of the SCLM (see discussion in text). Also shown are fresh MORBs (15) for comparison.

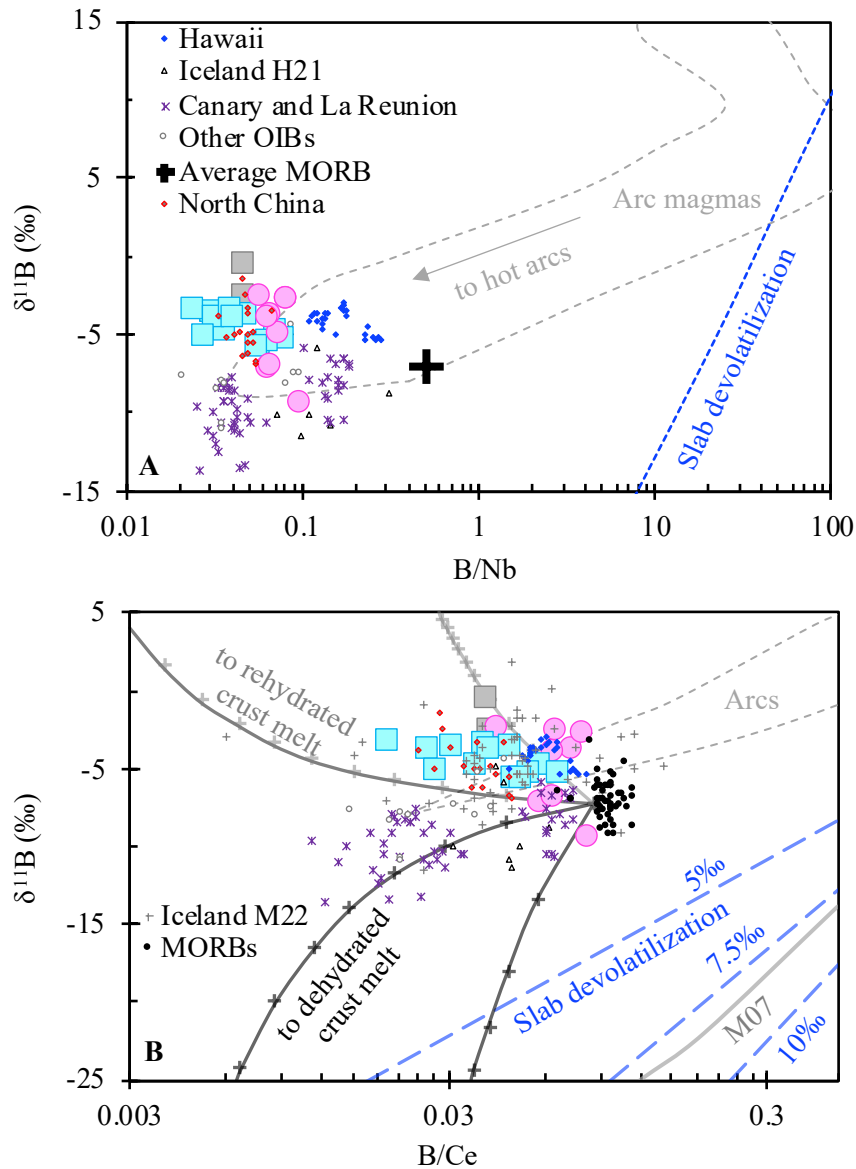


Fig. S3. $\delta^{11}\text{B}$ variation as a function of (A) Nb/B and (B) B/Ce for the studied samples. Also shown for comparison are data for MORBs (15), OIBs: Hawaii (110), La Palma (Canary Island) and Piton de Caille (La Reunion Island) (37), and other OIBs including Pitcairn Islands, Tristan da Cunha, St. Helena, Ascension Island, the MacDonal Sealamount, and Fogo (Cape Verde Islands) (36), Iceland (35, 38), and North China continental intraplate basalts (112). The field for arc magmas is from ref (24). The lines of slab devolatilization are taken from ref (76) in (a) and from ref (38) for three different fractionation factors ($\Delta^{11}\text{B}_{\text{fluid-solid}}$) and from ref (113) in (b). The two grey lines are mixing lines between rehydrated crust-derived melt with different B/Ce ratio and MORB, both are taken from ref (38). The two black lines are mixing lines between dehydrated crust-derived melt with different B/Ce ratio and $\delta^{11}\text{B}$ value and MORB, both are taken from ref (38).

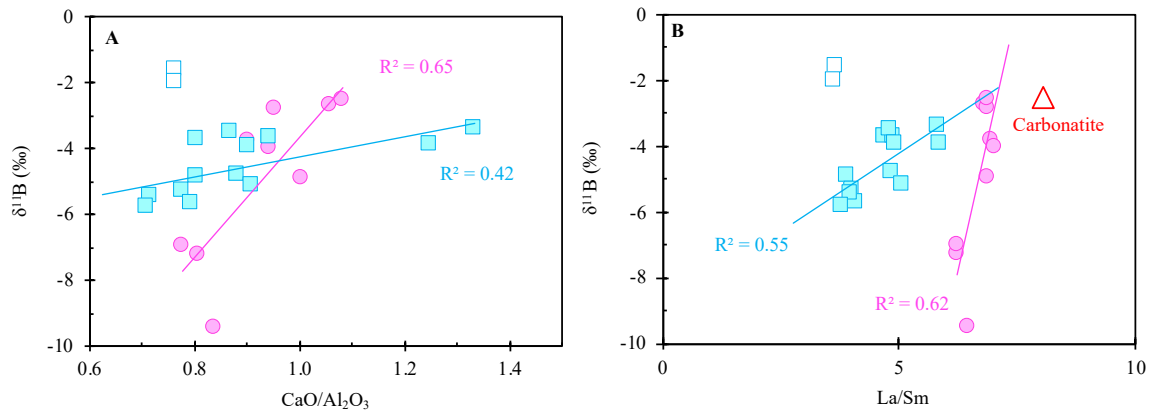


Fig. S4. $\delta^{11}\text{B}$ variation as a function of (A) $\text{CaO}/\text{Al}_2\text{O}_3$ and (B) La/Sm ratio for the studied samples. The best-fit regressions with R^2 values are shown. Symbols are as in Fig. S2. A carbonatite associated with recycled crustal carbon is shown (92).

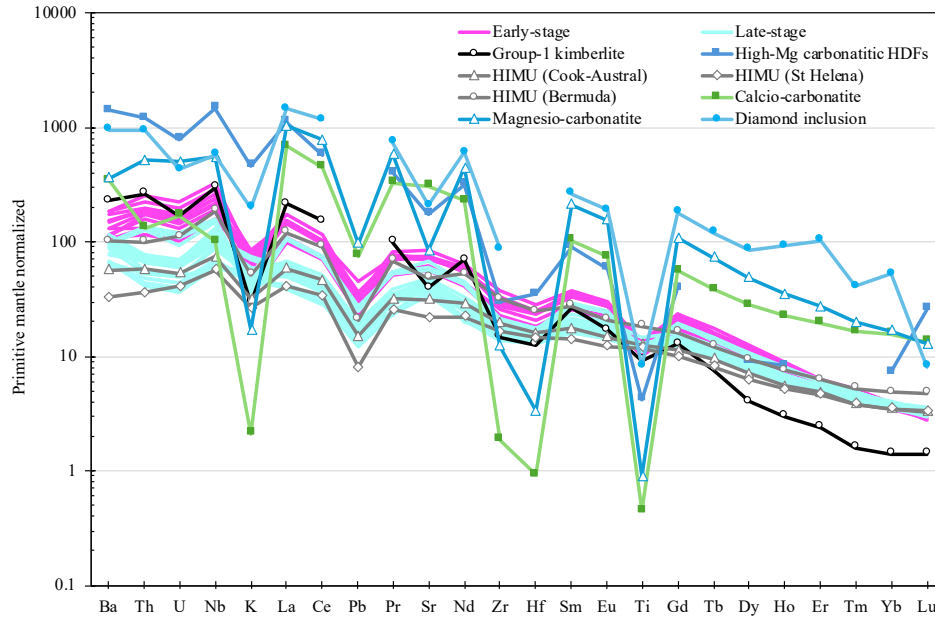


Fig. S5. Primitive mantle (114) normalized trace element patterns for our studied samples (40). Also shown for comparison are oceanic magnesio- and calcio-carbonatites (82), Group I kimberlites and high-Mg carbonate melts found in fluid inclusions within diamonds (83), deep diamond inclusion (11-ON-ZIZ) with HIMU-like incompatible trace element patterns (84), as well as typical oceanic HIMU basalts (85).

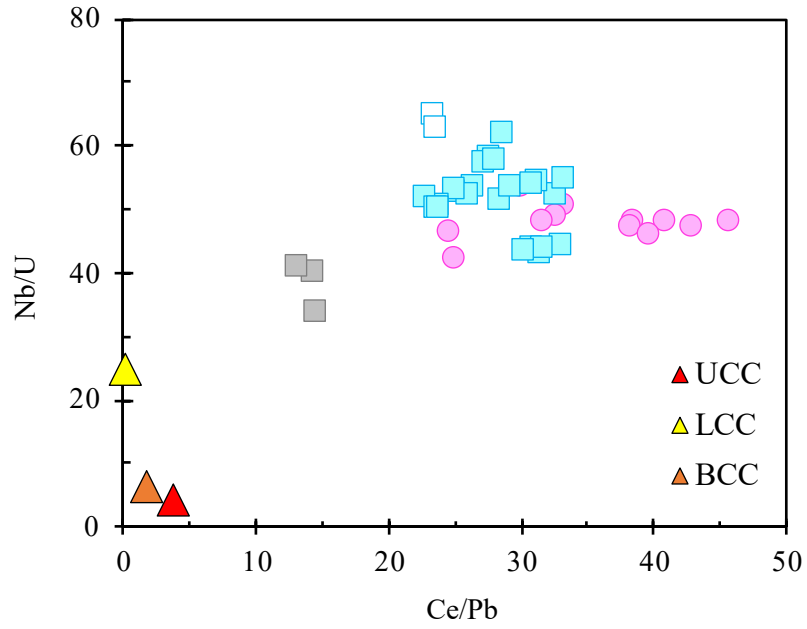


Figure S6. Nb/U versus Ce/Pb of the studied samples. Symbols are as in Fig. S2. The compositions for the lower (LCC), upper (UCC) and bulk (BCC) continental crust are from Rudnick and Gao (115).

Table S1. B content and isotope composition of the studied basalts and standards.

	Sample	B (ppm)	2SE	$\delta^{11}\text{B}$	2SE
Early-stage	18LY01	6.67	0.04	-7.25	0.25
	18LY01-R	5.04	0.03	-7.10	0.15
	18LY02	10.05	0.05	-9.46	0.19
	18LY03	7.99	0.04	-6.98	0.12
	18XL01	10.66	0.05	-4.91	0.11
	18XL02	12.30	0.06	-3.79	0.10
	18XL08	10.80	0.05	-3.99	0.12
	18XL09	11.21	0.06	-2.69	0.02
	18XL10	12.56	0.07	-2.81	0.23
	18XL11	7.22	0.04	-2.54	0.07
Late-stage	18XC01	2.82	0.02	-4.86	0.07
	18XC03	3.35	0.02	-5.30	0.10
	18XC05	2.41	0.02	-5.68	0.07
	18XC15	2.81	0.02	-5.42	0.33
	18XC16	2.54	0.02	-5.78	0.31
	18TT01	2.60	0.02	-3.67	0.02
	18TT01-R	2.59	0.01	-4.37	0.02
	18TT02	2.85	0.02	-4.78	0.08
	18TT03	1.77	0.01	-1.58	0.07
	18TT04	1.65	0.01	-1.98	0.09
	18TT12	2.40	0.01	-3.38	0.08
	18TT13	3.17	0.02	-3.88	0.07
	18SZ10	3.45	0.02	-3.71	0.08
	18SZ12	2.56	0.01	-3.47	0.08
	18SZ13	2.13	0.01	-5.14	0.08
	18SZ14	2.84	0.02	-3.91	0.09
	18SZ18	2.07	0.01	-0.55	0.08
	18SZ19	1.82	0.01	-2.56	0.02
	18SZ19-R	1.67	0.01	-3.41	0.01
	Standards				
Measured value	JB-2	31.11	0.16	7.15	0.09
Measured value	JB-2	29.16	0.16	7.32	0.24
Reference value	JB-2	30.00	0.90	7.21	0.41
Measured value	BCR-2	6.79	0.03	-3.73	0.14
Measured value	BCR-2	6.55	0.04	-4.43	0.16
Reference value	BCR-2	4.96	1.55	-5.92	0.02
Measured value	B5	12.08	0.06	-4.17	0.11
Measured value	B5	11.73	0.06	-3.91	0.12
Reference value	B5	9.74	1.09	-4.02	0.37
Measured value	seawater			39.56	0.10
Measured value	seawater			39.67	0.39
Reference value	seawater			39.6	0.2

Note: Reference values for JB-2, BCR-2 and B5 are from ref (116) and for seawater are from ref (107).

REFERENCES AND NOTES

1. R. Dasgupta, M. M. Hirschmann, The deep carbon cycle and melting in Earth's interior. *Earth Planet. Sci. Lett.* **298**, 1–13 (2010).
2. A. W. Hofmann, Mantle geochemistry: The message from oceanic volcanism. *Nature* **385**, 219–229 (1997).
3. W. M. White, Oceanic island basalts and mantle plumes: The geochemical perspective. *Annu. Rev. Earth Planet. Sci.* **38**, 133–160 (2010).
4. A. Zindler, S. Hart, Chemical geodynamics. *Annu. Rev. Earth Planet. Sci.* **14**, 493–571 (1986).
5. A. Stracke, Earth's heterogeneous mantle: A product of convection-driven interaction between crust and mantle. *Chem. Geol.* **330**, 274–299 (2012).
6. A. V. Sobolev, A. W. Hofmann, D. V. Kuzmin, G. M. Yaxley, N. T. Arndt, S. L. Chung, L. V. Danyushevsky, T. Elliott, F. A. Frey, M. O. Garcia, A. A. Gurenko, V. S. Kamenetsky, A. C. Kerr, N. A. Krivolutsкая, V. V. Matvienkov, I. K. Nikogosian, A. Rocholl, I. A. Sigurdsson, N. M. Sushchevskaya, M. Teklay, The amount of recycled crust in sources of mantle-derived melts. *Science* **316**, 412–417 (2007).
7. Y. Niu, M. Wilson, E. R. Humphreys, M. J. O'Hara, The origin of intra-plate ocean island basalts (OIB): The lid effect and its geodynamic implications. *J. Petrol.* **52**, 1443–1468 (2011).
8. R. Dasgupta, M. M. Hirschmann, Melting in the Earth's deep upper mantle caused by carbon dioxide. *Nature* **440**, 659–662 (2006).
9. J. M. Brenan, E. B. Watson, Partitioning of trace elements between carbonate melt and clinopyroxene and olivine at mantle *P-T* conditions. *Geochim. Cosmochim. Acta* **55**, 2203–2214 (1991).
10. J. M. Brenan, E. B. Watson, Partitioning of trace elements between olivine and aqueous fluids at high *P-T* conditions: Implications for the effect of fluid composition on trace-element transport. *Earth Planet. Sci. Lett.* **107**, 672–688 (1991).

11. X.-J. Wang, L.-H. Chen, A. W. Hofmann, T. Hanyu, H. Kawabata, Y. Zhong, L.-W. Xie, J.-H. Shi, T. Miyazaki, Y. Hirahara, T. Takahashi, R. Senda, Q. Chang, B. S. Vaglarov, J.-I. Kimura, Recycled ancient ghost carbonate in the Pitcairn mantle plume. *Proc. Natl. Acad. Sci. U.S.A.* **115**, 8682–8687 (2018).
12. Z. Wang, Z. Zhang, M. K. Reichow, W. Tian, W. Kong, B. Liu, Tracing decarbonated eclogite in the mantle sources of Tarim continental flood basalts using Zn isotopes. *Geol. Soc. Am. Bull.* **135**, 1768–1782 (2023).
13. Q. Xie, Z. Zhang, S. F. Foley, C. Chen, Z. Cheng, Y. Wang, W. Kong, Y. Lv, M. Santosh, Q. Jin, Transition from tholeiitic to alkali basalts via interaction between decarbonated eclogite-derived melts and peridotite. *Chem. Geol.* **621**, 121354 (2023).
14. S.-J. Wang, F.-Z. Teng, S.-G. Li, Tracing carbonate–silicate interaction during subduction using magnesium and oxygen isotopes. *Nat. Commun.* **5**, 5328 (2014).
15. H. R. Marschall, V. D. Wanless, N. Shimizu, P. A. P. von Strandmann, T. Elliott, B. D. Monteleone, The boron and lithium isotopic composition of mid-ocean ridge basalts and the mantle. *Geochim. Cosmochim. Acta* **207**, 102–138 (2017).
16. H.-Y. Li, X. Li, J. G. Ryan, C. Zhang, Y.-G. Xu, Boron isotopes in boninites document rapid changes in slab inputs during subduction initiation. *Nat. Commun.* **13**, 993 (2022).
17. G. F. Cooper, C. G. Macpherson, J. D. Blundy, B. Maunder, R. W. Allen, S. Goes, J. S. Collier, L. Bie, N. Harmon, S. P. Hicks, A. A. Iveson, J. Prytulak, A. Rietbrock, C. A. Rychert, J. P. Davidson, the VoiLA team, Variable water input controls evolution of the Lesser Antilles volcanic arc. *Nature* **582**, 525–529 (2020).
18. M. R. Palmer, G. H. Swihart, Boron isotope geochemistry: An overview. *Rev. Mineral. Geochem.* **33**, 709–744 (1996).
19. R. L. Hervig, G. M. Moore, L. B. Williams, S. M. Peacock, J. R. Holloway, K. Roggensack, Isotopic and elemental partitioning of boron between hydrous fluid and silicate melt. *Am. Mineral.* **87**, 769–774 (2002).

20. C. Schmidt, R. Thomas, W. Heinrich, Boron speciation in aqueous fluids at 22 to 600°C and 0.1 MPa to 2 GPa. *Geochim. Cosmochim. Acta* **69**, 275–281 (2005).
21. W. P. Leeman, S. Tonarini, L. H. Chan, L. E. Borg, Boron and lithium isotopic variations in a hot subduction zone—The southern Washington Cascades. *Chem. Geol.* **212**, 101–124 (2004).
22. M. Rosner, J. Erzinger, G. Franz, R. B. Trumbull, Slab-derived boron isotope signatures in arc volcanic rocks from the Central Andes and evidence for boron isotope fractionation during progressive slab dehydration. *Geochem. Geophys. Geosyst.* **4**, 9005 (2003).
23. S. Tonarini, W. P. Leeman, P. T. Leat, Subduction erosion of forearc mantle wedge implicated in the genesis of the South Sandwich Island (SSI) arc: Evidence from boron isotope systematics. *Earth Planet. Sci. Lett.* **301**, 275–284 (2011).
24. J. C. M. De Hoog, I. P. Savov, “Boron isotopes as a tracer of subduction zone processes” in *Boron Isotopes: The Fifth Element*, H. Marschall, G. Foster, Eds. (Springer, 2018), chap. 9, pp. 217–247.
25. Y. Yu, X.-L. Huang, M. Sun, J.-L. Ma, B isotopic constraints on the role of H₂O in mantle wedge melting. *Geochim. Cosmochim. Acta* **303**, 92–109 (2021).
26. P.-P. Liu, D.-B. Wang, M.-F. Zhou, X.-H. Li, Q.-L. Li, G. A. Gaetani, B. Monteleone, V. Kamenetsky, Constraints of boron and oxygen stable isotopes on dehydration fluids, sediment-derived melts, and crustal assimilation of the Toba volcanic system (Indonesia). *Geology* **52**, 161–165 (2023).
27. D. Wang, R. L. Romer, J.-h. Guo, J. Glodny, Li and B isotopic fingerprint of Archean subduction. *Geochim. Cosmochim. Acta* **268**, 446–466 (2020).
28. T. Ishikawa, E. Nakamura, Boron isotope systematics of marine sediments. *Earth Planet. Sci. Lett.* **117**, 567–580 (1993).
29. N. G. Hemming, G. N. Hanson, Boron isotopic composition and concentration in modern marine carbonates. *Geochim. Cosmochim. Acta* **56**, 537–543 (1992).

30. A. Vengosh, Y. Kolodny, A. Starinsky, A. R. Chivas, M. T. McCulloch, Coprecipitation and isotopic fractionation of boron in modern biogenic carbonates. *Geochim. Cosmochim. Acta* **55**, 2901–2910 (1991).
31. S. Zhang, M. J. Henehan, P. M. Hull, R. P. Reid, D. S. Hardisty, A. v. S. Hood, N. J. Planavsky, Investigating controls on boron isotope ratios in shallow marine carbonates. *Earth Planet. Sci. Lett.* **458**, 380–393 (2017).
32. Y. Zhang, C. Yuan, M. Sun, J. Li, X. Long, Y. Jiang, Z. Huang, Molybdenum and boron isotopic evidence for carbon-recycling via carbonate dissolution in subduction zones. *Geochim. Cosmochim. Acta* **278**, 340–352 (2020).
33. X.-Y. Zhang, L.-H. Chen, X.-J. Wang, T. Hanyu, A. W. Hofmann, T. Komiya, K. Nakamura, Y. Kato, G. Zeng, W.-X. Gou, W.-Q. Li, Zinc isotopic evidence for recycled carbonate in the deep mantle. *Nat. Commun.* **13**, 6085 (2022).
34. A. J. Spivack, J. M. Edmond, Boron isotope exchange between seawater and the oceanic crust. *Geochim. Cosmochim. Acta* **51**, 1033–1043 (1987).
35. M. E. Hartley, J. C. M. de Hoog, O. Shorttle, Boron isotopic signatures of melt inclusions from North Iceland reveal recycled material in the Icelandic mantle source. *Geochim. Cosmochim. Acta* **294**, 273–294 (2021).
36. K. J. Walowski, L. A. Kirstein, J. C. M. De Hoog, T. Elliott, I. P. Savov, R. E. Jones, EIMF, Boron recycling in the mantle: Evidence from a global comparison of ocean island basalts. *Geochim. Cosmochim. Acta* **302**, 83–100 (2021).
37. K. J. Walowski, L. A. Kirstein, J. C. M. De Hoog, T. R. Elliott, I. P. Savov, R. E. Jones, Investigating ocean island mantle source heterogeneity with boron isotopes in melt inclusions. *Earth Planet. Sci. Lett.* **508**, 97–108 (2019).
38. E. W. Marshall, E. Ranta, S. A. Halldórsson, A. Caracciolo, E. Bali, H. Jeon, M. J. Whitehouse, J. D. Barnes, A. Stefánsson, Boron isotope evidence for devolatilized and

- rehydrated recycled materials in the Icelandic mantle source. *Earth Planet. Sci. Lett.* **577**, 117229 (2022).
39. J. Aggarwal, M. Palmer, T. D. Bullen, S. Arnórsson, K. Ragnarsdóttir, The boron isotope systematics of Icelandic geothermal waters: 1. Meteoric water charged systems. *Geochim. Cosmochim. Acta* **64**, 579–585 (2000).
40. R. Xu, Y. Liu, S. Lambart, K. Hoernle, Y. Zhu, Z. Zou, J. Zhang, Z. Wang, M. Li, F. Moynier, K. Zong, H. Chen, Z. Hu, Decoupled Zn-Sr-Nd isotopic composition of continental intraplate basalts caused by two-stage melting process. *Geochim. Cosmochim. Acta* **326**, 234–252 (2022).
41. R. Xu, S. Lambart, O. Nebel, M. Li, Z. Bai, J. Zhang, G. Zhang, J. Gao, H. Zhong, Y. Liu, Iron isotope evidence in continental intraplate basalts for mantle lithosphere imprint on heterogeneous asthenospheric melts. *Earth Planet. Sci. Lett.* **625**, 118499 (2024).
42. K. Ho, J. Chen, C. Lo, H. Zhao, ^{40}Ar – ^{39}Ar dating and geochemical characteristics of late Cenozoic basaltic rocks from the Zhejiang–Fujian region, SE China: Eruption ages, magma evolution and petrogenesis. *Chem. Geol.* **197**, 287–318 (2003).
43. S.-C. Liu, Q.-K. Xia, S. H. Choi, E. Deloule, P. Li, J. Liu, Continuous supply of recycled Pacific oceanic materials in the source of Cenozoic basalts in SE China: The Zhejiang case. *Contrib. Mineral. Petrol.* **171**, 100 (2016).
44. Y.-Q. Li, C.-Q. Ma, P. T. Robinson, Q. Zhou, M.-L. Liu, Recycling of oceanic crust from a stagnant slab in the mantle transition zone: Evidence from Cenozoic continental basalts in Zhejiang Province, SE China. *Lithos* **230**, 146–165 (2015).
45. X. Yu, L.-H. Chen, G. Zeng, Growing magma chambers control the distribution of small-scale flood basalts. *Sci. Rep.* **5**, 16824 (2015).
46. J. Huang, D. Zhao, High-resolution mantle tomography of China and surrounding regions. *J. Geophys. Res.* **111**, B09305 (2006).

47. Y. Xu, H. Li, L. Hong, L. Ma, Q. Ma, M. Sun, Generation of Cenozoic intraplate basalts in the big mantle wedge under eastern Asia. *Sci. China Earth Sci.* **61**, 869–886 (2018).
48. S.-G. Li, W. Yang, S. Ke, X. Meng, H. Tian, L. Xu, Y. He, J. Huang, X.-C. Wang, Q. Xia, W. Sun, X. Yang, Z.-Y. Ren, H. Wei, Y. Liu, F. Meng, J. Yan, Deep carbon cycles constrained by a large-scale mantle Mg isotope anomaly in eastern China. *Nat. Sci. Rev.* **4**, 111–120 (2017).
49. R. Xu, Y. Liu, X.-C. Wang, S. F. Foley, Y. Zhang, H. Yuan, Generation of continental intraplate alkali basalts and implications for deep carbon cycle. *Earth Sci. Rev.* **201**, 103073 (2020).
50. G. Zeng, L.-H. Chen, A. W. Hofmann, X.-J. Wang, J.-Q. Liu, X. Yu, L.-W. Xie, Nephelinites in eastern China originating from the mantle transition zone. *Chem. Geol.* **576**, 120276 (2021).
51. X.-H. Dong, S.-J. Wang, W. Wang, S. Huang, Q.-L. Li, C. Liu, T. Gao, S. Li, S. Wu, Highly oxidized intraplate basalts and deep carbon storage. *Sci. Adv.* **10**, eadm8138 (2024).
52. A. Gale, C. A. Dalton, C. H. Langmuir, Y. Su, J.-G. Schilling, The mean composition of ocean ridge basalts. *Geochem. Geophys. Geosyst.* **14**, 489–518 (2013).
53. J. Liu, Z.-Z. Wang, H.-R. Yu, Q.-K. Xia, E. Deloule, M. Feng, Dynamic contribution of recycled components from the subducted Pacific slab: Oxygen isotopic composition of the basalts from 106 Ma to 60 Ma in North China Craton. *J. Geophys. Res. Solid Earth* **122**, 988–1006 (2017).
54. Y.-G. Xu, H.-H. Zhang, H.-N. Qiu, W.-C. Ge, F.-Y. Wu, Oceanic crust components in continental basalts from Shuangliao, Northeast China: Derived from the mantle transition zone? *Chem. Geol.* **328**, 168–184 (2012).
55. H.-Y. Li, Y.-G. Xu, J. G. Ryan, X.-L. Huang, Z.-Y. Ren, H. Guo, Z.-G. Ning, Olivine and melt inclusion chemical constraints on the source of intracontinental basalts from the eastern North China Craton: Discrimination of contributions from the subducted Pacific slab. *Geochim. Cosmochim. Acta* **178**, 1–19 (2016).

56. R. Xu, Y. Liu, X. Wang, K. Zong, Z. Hu, H. Chen, L. Zhou, Crust recycling induced compositional-temporal-spatial variations of Cenozoic basalts in the Trans-North China Orogen. *Lithos* **274**, 383–396 (2017).
57. W. Fang, L.-Q. Dai, Y.-F. Zheng, Z.-F. Zhao, Molybdenum isotopes in mafic igneous rocks record slabmantle interactions from subarc to postarc depths. *Geology* **51**, 3–7 (2023).
58. J.-Q. Liu, Z.-Y. Ren, A. R. L. Nichols, M.-S. Song, S.-P. Qian, Y. Zhang, P.-P. Zhao, Petrogenesis of Late Cenozoic basalts from North Hainan Island: Constraints from melt inclusions and their host olivines. *Geochim. Cosmochim. Acta* **152**, 89–121 (2015).
59. J. Liu, Q.-K. Xia, E. Deloule, H. Chen, M. Feng, Recycled oceanic crust and marine sediment in the source of alkali basalts in Shandong, eastern China: Evidence from magma water content and oxygen isotopes. *J. Geophys. Res. Solid Earth* **120**, 8281–8303 (2015).
60. J. Liu, Q.-K. Xia, E. Deloule, J. Ingrin, H. Chen, M. Feng, Water content and oxygen isotopic composition of alkali basalts from the Taihang Mountains, China: Recycled oceanic components in the mantle source. *J. Petrol.* **56**, 681–702 (2015).
61. Z. Zou, Z. Wang, S. Foley, R. Xu, X. Geng, Y.-N. Liu, Y. Liu, Z. Hu, Origin of low-MgO primitive intraplate alkaline basalts from partial melting of carbonate-bearing eclogite sources. *Geochim. Cosmochim. Acta* **324**, 240–261 (2022).
62. H.-K. Dai, J.-P. Zheng, S. Y. O'Reilly, W. L. Griffin, Q. Xiong, R. Xu, Y.-P. Su, X.-Q. Ping, F.-K. Chen, Langshan basalts record recycled Paleo-Asian oceanic materials beneath the northwest North China Craton. *Chem. Geol.* **524**, 88–103 (2019).
63. T. Sakuyama, W. Tian, J.-I. Kimura, Y. Fukao, Y. Hirahara, T. Takahashi, R. Senda, Q. Chang, T. Miyazaki, M. Obayashi, H. Kawabata, Y. Tatsumi, Melting of dehydrated oceanic crust from the stagnant slab and of the hydrated mantle transition zone: Constraints from Cenozoic alkaline basalts in eastern China. *Chem. Geol.* **359**, 32–48 (2013).

64. H. Chen, Q.-K. Xia, J. Ingrin, E. Deloule, Y. Bi, Heterogeneous source components of intraplate basalts from NE China induced by the ongoing Pacific slab subduction. *Earth Planet. Sci. Lett.* **459**, 208–220 (2017).
65. S.-P. Qian, Z.-Y. Ren, L. Zhang, L.-B. Hong, J.-Q. Liu, Chemical and Pb isotope composition of olivine-hosted melt inclusions from the Hannuoba basalts, North China Craton: Implications for petrogenesis and mantle source. *Chem. Geol.* **401**, 111–125 (2015).
66. G. Zeng, L.-H. Chen, X. Yu, J.-Q. Liu, X.-S. Xu, S. Erdmann, Magma-magma interaction in the mantle beneath eastern China. *J. Geophys. Res. Solid Earth* **122**, 2763–2779 (2017).
67. S.-Y. Yu, Y.-G. Xu, K.-J. Huang, J.-B. Lan, L.-M. Chen, S.-H. Zhou, Magnesium isotope constraints on contributions of recycled oceanic crust and lithospheric mantle to generation of intraplate basalts in a big mantle wedge. *Lithos* **398-399**, 106327 (2021).
68. X. Yu, G. Zeng, L.-H. Chen, X.-J. Wang, J.-Q. Liu, L.-W. Xie, T. Yang, Evidence for rutile-bearing eclogite in the mantle sources of the Cenozoic Zhejiang basalts, eastern China. *Lithos* **324-325**, 152–164 (2019).
69. H.-L. Zhang, G. Zeng, J.-Q. Liu, L.-H. Chen, J.-H. Yu, B. Wu, X.-J. Wang, X.-S. Xu, X.-W. Liu, Carbonated eclogitic component beneath eastern China revealed by olivine phenocrysts in nephelinites. *Chem. Geol.* **640**, 121744 (2023).
70. Z. Wei, H. Y. Li, L. Ma, Y.-S. Hou, Y. Wang, Y.-G. Xu, Geochemistry of olivine melt inclusion reveals interactions between deeply derived carbonated melts from the big mantle Wedge and Pyroxenite in the lithospheric mantle beneath Eastern Asia. *Geophys. Res. Lett.* **51**, e2024GL108234 (2024).
71. F.-B. Pan, C. Jin, X. He, L. Tao, B.-J. Jia, A plate-mantle convection system in the West Pacific revealed by tertiary ultramafic-mafic volcanic rocks in Southeast China. *Earth Space Sci.* **8**, e2020EA001324 (2021).
72. J. E. Dixon, L. Leist, C. Langmuir, J.-G. Schilling, Recycled dehydrated lithosphere observed in plume-influenced mid-ocean-ridge basalt. *Nature* **420**, 385–389 (2002).

73. T. Plank, “The chemical composition of subducting sediments” in *Treatise on Geochemistry*, H. D. Holland, K. K. Turekian, Eds. (Elsevier, 2014), vol. 4, pp. 607–629.
74. G. E. Bebout, E. Nakamura, Record in metamorphic tourmalines of subduction-zone devolatilization and boron cycling. *Geology* **31**, 407–410 (2003).
75. D. M. Saffer, A. J. Kopf, Boron desorption and fractionation in Subduction Zone Fore Arcs: Implications for the sources and transport of deep fluids. *Geochem. Geophys. Geosyst.* **17**, 4992–5008 (2016).
76. P. J. Sugden, I. P. Savov, S. Agostini, M. Wilson, R. Halama, K. Meliksetian, Boron isotope insights into the origin of subduction signatures in continent-continent collision zone volcanism. *Earth Planet. Sci. Lett.* **538**, 116207 (2020).
77. L.-L. Hao, Q. Wang, A. C. Kerr, G.-J. Wei, F. Huang, M.-Y. Zhang, Y. Qi, L. Ma, X.-F. Chen, Y.-N. Yang, Contribution of continental subduction to very light B isotope signatures in post-collisional magmas: Evidence from southern Tibetan ultrapotassic rocks. *Earth Planet. Sci. Lett.* **584**, 117508 (2022).
78. M. Tatsumoto, A. R. Basu, H. Wankang, W. Junwen, X. Guanghong, Sr, Nd, and Pb isotopes of ultramafic xenoliths in volcanic rocks of Eastern China: Enriched components EMI and EMII in subcontinental lithosphere. *Earth Planet. Sci. Lett.* **113**, 107–128 (1992).
79. H. Zou, A. Zindler, X. Xu, Q. Qi, Major, trace element, and Nd, Sr and Pb isotope studies of Cenozoic basalts in SE China: Mantle sources, regional variations, and tectonic significance. *Chem. Geol.* **171**, 33–47 (2000).
80. F. Guo, Y. Wu, B. Zhang, X. Zhang, L. Zhao, J. Liao, Magmatic responses to Cretaceous subduction and tearing of the paleo-Pacific Plate in SE China: An overview. *Earth Sci. Rev.* **212**, 103448 (2021).
81. M. R. Guild, “Boron isotopic composition of the subcontinental lithospheric mantle,” thesis, Arizona State University (2014).

82. K. Hoernle, G. Tilton, M. J. Le Bas, S. Duggen, D. Garbe-Schönberg, Geochemistry of oceanic carbonatites compared with continental carbonatites: Mantle recycling of oceanic crustal carbonate. *Contrib. Mineral. Petrol.* **142**, 520–542 (2002).
83. Y. Weiss, W. L. Griffin, D. R. Bell, O. Navon, High-Mg carbonatitic melts in diamonds, kimberlites and the sub-continental lithosphere. *Earth Planet. Sci. Lett.* **309**, 337–347 (2011).
84. S. Huang, O. Tschauer, S. Yang, M. Humayun, W. Liu, S. N. Gilbert Corder, H. A. Bechtel, J. Tischler, HIMU geochemical signature originating from the transition zone. *Earth Planet. Sci. Lett.* **542**, 116323 (2020).
85. S. E. Mazza, E. Gazel, M. Bizimis, R. Moucha, P. Béguelin, E. A. Johnson, R. J. McAleer, A. V. Sobolev, Sampling the volatile-rich transition zone beneath Bermuda. *Nature* **569**, 398–403 (2019).
86. R. Dasgupta, M. M. Hirschmann, W. F. McDonough, M. Spiegelman, A. C. Withers, Trace element partitioning between garnet lherzolite and carbonatite at 6.6 and 8.6 GPa with applications to the geochemistry of the mantle and of mantle-derived melts. *Chem. Geol.* **262**, 57–77 (2009).
87. J. Huang, S.-G. Li, Y. Xiao, S. Ke, W.-Y. Li, Y. Tian, Origin of low $\delta^{26}\text{Mg}$ Cenozoic basalts from South China Block and their geodynamic implications. *Geochim. Cosmochim. Acta* **164**, 298–317 (2015).
88. Q.-Z. Jin, J. Huang, S.-C. Liu, F. Huang, Magnesium and zinc isotope evidence for recycled sediments and oceanic crust in the mantle sources of continental basalts from eastern China. *Lithos* **370-371**, 105627 (2020).
89. S.-A. Liu, Z.-Z. Wang, S.-G. Li, J. Huang, W. Yang, Zinc isotope evidence for a large-scale carbonated mantle beneath eastern China. *Earth Planet. Sci. Lett.* **444**, 169–178 (2016).
90. H. Beunon, N. Mattielli, L. S. Doucet, B. Moine, B. Debret, Mantle heterogeneity through Zn systematics in oceanic basalts: Evidence for a deep carbon cycling. *Earth Sci. Rev.* **205**, 103174 (2020).

91. S. R. W. Hulett, A. Simonetti, E. T. Rasbury, N. G. Hemming, Recycling of subducted crustal components into carbonatite melts revealed by boron isotopes. *Nat. Geosci.* **9**, 904–908 (2016).
92. O. Çimen, C. Kuebler, S. S. Simonetti, L. Corcoran, R. Mitchell, A. Simonetti, Combined boron, radiogenic (Nd, Pb, Sr), stable (C, O) isotopic and geochemical investigations of carbonatites from the Blue River Region, British Columbia (Canada): Implications for mantle sources and recycling of crustal carbon. *Chem. Geol.* **529**, 119240 (2019).
93. J. E. Dixon, I. N. Bindeman, R. H. Kingsley, K. K. Simons, P. J. Le Roux, T. R. Hajewski, P. Swart, C. H. Langmuir, J. G. Ryan, K. J. Walowski, I. Wada, P. J. Wallace, Light stable isotopic compositions of enriched mantle sources: Resolving the dehydration paradox. *Geochem. Geophys. Geosyst.* **18**, 3801–3839 (2017).
94. F.-Z. Teng, W.-Y. Li, S. Ke, B. Marty, N. Dauphas, S. Huang, F.-Y. Wu, A. Pourmand, Magnesium isotopic composition of the Earth and chondrites. *Geochim. Cosmochim. Acta* **74**, 4150–4166 (2010).
95. X.-Y. Qiao, J.-W. Xiong, Y.-X. Chen, J. C. De Hoog, J. Pearce, F. Huang, Z.-F. Zhao, K. Chen, Magnesium and boron isotope evidence for the generation of arc magma through serpentinite mélange melting. *Nat. Sci. Rev.* **12**, nwae363 (2025).
96. M. E. Regier, K. V. Smit, T. B. Chalk, T. Stachel, R. A. Stern, E. M. Smith, G. L. Foster, Y. Bussweiler, C. DeBuhr, A. D. Burnham, J. W. Harris, D. G. Pearson, Boron isotopes in blue diamond record seawater-derived fluids in the lower mantle. *Earth Planet. Sci. Lett.* **602**, 117923 (2023).
97. P. B. Kelemen, C. E. Manning, Reevaluating carbon fluxes in subduction zones, what goes down, mostly comes up. *Proc. Natl. Acad. Sci. U.S.A.* **112**, E3997–E4006 (2015).
98. T. Plank, C. E. Manning, Subducting carbon. *Nature* **574**, 343–352 (2019).
99. N. Coltice, L. Simon, C. Lécuyer, Carbon isotope cycle and mantle structure. *Geophys. Res. Lett.* **31**, L05603 (2004).

100. A. R. Thomson, M. J. Walter, S. C. Kohn, R. A. Brooker, Slab melting as a barrier to deep carbon subduction. *Nature* **529**, 76–79 (2016).
101. M. Ichiki, K. Baba, M. Obayashi, H. Utada, Water content and geotherm in the upper mantle above the stagnant slab: Interpretation of electrical conductivity and seismic P-wave velocity models. *Phys. Earth Planet. Inter.* **155**, 1–15 (2006).
102. Q.-K. Xia, J. Liu, I. Kovács, Y.-T. Hao, P. Li, X.-Z. Yang, H. Chen, Y.-M. Sheng, Water in the upper mantle and deep crust of eastern China: Concentration, distribution and implications. *Nat. Sci. Rev.* **6**, 125–144 (2019).
103. X.-C. Wang, S. A. Wilde, Q.-L. Li, Y.-N. Yang, Continental flood basalts derived from the hydrous mantle transition zone. *Nat. Commun.* **6**, 7700 (2015).
104. T. Kuritani, E. Ohtani, J.-I. Kimura, Intensive hydration of the mantle transition zone beneath China caused by ancient slab stagnation. *Nat. Geosci.* **4**, 713–716 (2011).
105. K.-C. Xing, F. Wang, F.-Z. Teng, W.-L. Xu, Y.-N. Wang, D.-B. Yang, H.-L. Li, Y.-C. Wang, Potassium isotopic evidence for recycling of surface water into the mantle transition zone. *Nat. Geosci.* **17**, 579–585 (2024).
106. J. Yang, M. Faccenda, Intraplate volcanism originating from upwelling hydrous mantle transition zone. *Nature* **579**, 88–91 (2020).
107. Y. Cai, T. Ruan, Y. Li, B. Li, W. Zhang, Z. Li, H. Wei, E. T. Rasbury, Improved alkaline fusion method for B isotope and concentration measurements of silicate materials. *J. Anal. At. Spectrom.* **38**, 1934–1942 (2023).
108. M. Chaussidon, F. Albarède, Secular boron isotope variations in the continental crust: An ion microprobe study. *Earth Planet. Sci. Lett.* **108**, 229–241 (1992).
109. R. B. Trumbull, J. F. Slack, “Boron isotopes in the continental crust: granites, pegmatites, felsic volcanic rocks, and related ore deposits” in *Boron Isotopes: The Fifth Element*, H. Marschall, G. Foster, Eds. (Springer, 2018), chap. 10, pp. 249-272.

110. R. Tanaka, E. Nakamura, Boron isotopic constraints on the source of Hawaiian shield lavas. *Geochim. Cosmochim. Acta* **69**, 3385–3399 (2005).
111. J. Liu, C. Tao, J. Zhou, K. Shimizu, W. Li, J. Liang, S. Liao, T. Kuritani, E. Deloule, T. Ushikubo, M. Nakagawa, W. Yang, G. Zhang, Y. Liu, C. Zhu, H. Sun, J. Zhou, Water enrichment in the mid-ocean ridge by recycling of mantle wedge residue. *Earth Planet. Sci. Lett.* **584**, 117455 (2022).
112. H.-Y. Li, Z. Zhou, J. G. Ryan, G.-J. Wei, Y.-G. Xu, Boron isotopes reveal multiple metasomatic events in the mantle beneath the eastern North China Craton. *Geochim. Cosmochim. Acta* **194**, 77–90 (2016).
113. H. R. Marschall, R. Altherr, L. Rüpke, Squeezing out the slab — Modelling the release of Li, Be and B during progressive high-pressure metamorphism. *Chem. Geol.* **239**, 323–335 (2007).
114. W. F. McDonough, S.-s. Sun, The composition of the Earth. *Chem. Geol.* **120**, 223–253 (1995).
115. R. L. Rudnick, S. Gao, “Composition of the continental crust” in *Treatise on Geochemistry*, H. D. Holland, K. K. Turekian, Eds. (Elsevier, 2003), vol. 3, pp. 1–64.
116. G. Zhu, J. Ma, G. Wei, L. Zhang, Boron mass fractions and $\delta^{11}\text{B}$ values of eighteen international geological reference materials. *Geostand. Geoanalytical Res.* **45**, 583–598 (2021).